This pdf file consists of figures containing photographs, and their captions, scanned from:

THE DEVELOPMENT OF FOLIATIONS IN LOW, MEDIUM AND HIGH GRADE METAMORPHIC TECTONITES

by

William J. Gregg

A Dissertation

Submitted to the State University of New York at Albany

in partial fulfillment of

the requirements for the degree of

Doctor of Philosophy

College of Arts and Sciences

Department of Geological Sciences

1979

Figure 1.3 - Typical example of B_1 folds in a siltstone-dominated sequence near the bench mark (BM) at Turtle Head. Cleavage is well developed as a convergent axial surface fan in the siltstone beds and is composed of fine scale secondary layering and discrete mica films. The open to close degree of folding is typical of B_1 styles in siltstones. Pelitic units between siltstone beds are about 5 mm thick or less. The siltstone beds are from 10 to 50 mm thick.

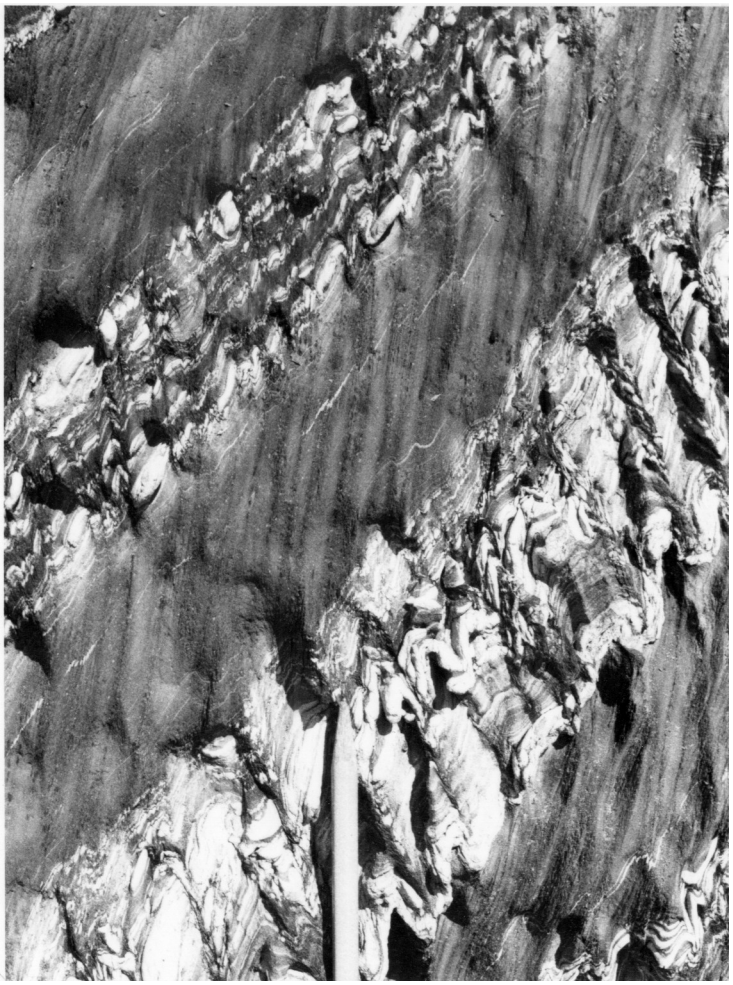

Figure 1.7 - a) a typical example from a pelite-dominated sequence showing B_1 mesoscopic folds in siltstone beds on all scales and well developed cleavage in the pelite continuous with the more "differentiated" and refracted cleavage in the siltstone beds. Cross bedding is usually easy to recognize even on this scale in the field. Note the absence of a second cleavage attributable to B_2. This lack of S_2 development is common in all but one small locality at Turtle Head.

Figure 1.8 - Mesoscopic style group T-1 structures developed in pelite-dominated sequences.

a) Detailed illustration of bedding traces shown previously in figure 1.7. The fine silty lamination is about .5 mm thick. These beds are commonly discontinuous because they originated as cross-bedded fillings of small, shallow sedimentary troughs. Fine S_1 cleavage is visible and the absence of any overprinting foliation is noteworthy. This example as well as the following examples are from the coastline to the south of "the neck."

b) S_1 cleavage is depicted and refraction of cleavage in silty beds is illustrated.

c) In this example S_1 cleavage is shown in a sequence containing more abundant siltstone layers.

d) This specimen from locality 177 (west coastal section) illustrates local transposition of layering in a thin pelite bed enclosed between two thick siltstone beds. There is much internal deformation in the pelite whereas the siltstone beds display only a fine S_1 cleavage.

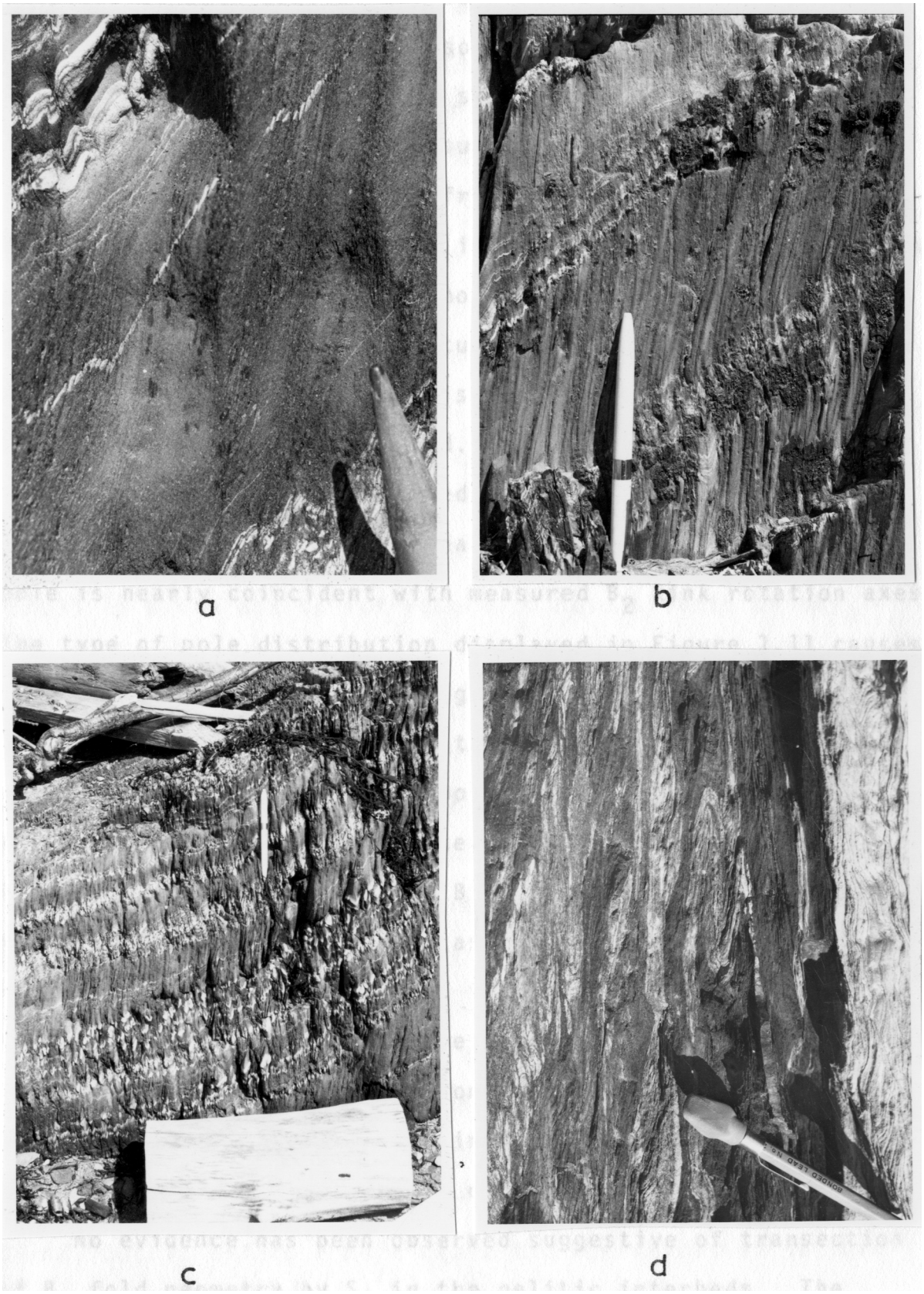

Fig. 1.8

Figure 1.9 - Mesoscopic style group T-1 structures in interbedded pelite-siltstone units.

a) Fine S_1 cleavage at locality 139 (west coastal section). A number of irregular trough-like structures can be seen in the silty beds. A small cleavage-parallel, discontinuous fault is shown in the lower left hand corner. These rocks are cut by S_2 cleavage which is not apparent on this scale of observation (see figure 1.15).

b) Strongly refracted S_1 cleavage from the coastal section south of "the neck."

c) Detail of a specimen collected by W.D. Means from a locality south of "the neck" illustrating fine S_1 cleavage and offsets of S_0 which appear to record evidence of shear displacement on S_1. The width of the photograph is about 20 mm.

d) Thin section view of thick S_1 layer in silty bed showing concentration of opaque minerals in the vertically oriented S_1 mica-rich layer. Open fractures are artifacts of the thin sectioning process. Specimen S-84a. Width of mica-rich layer is about 7 mm.

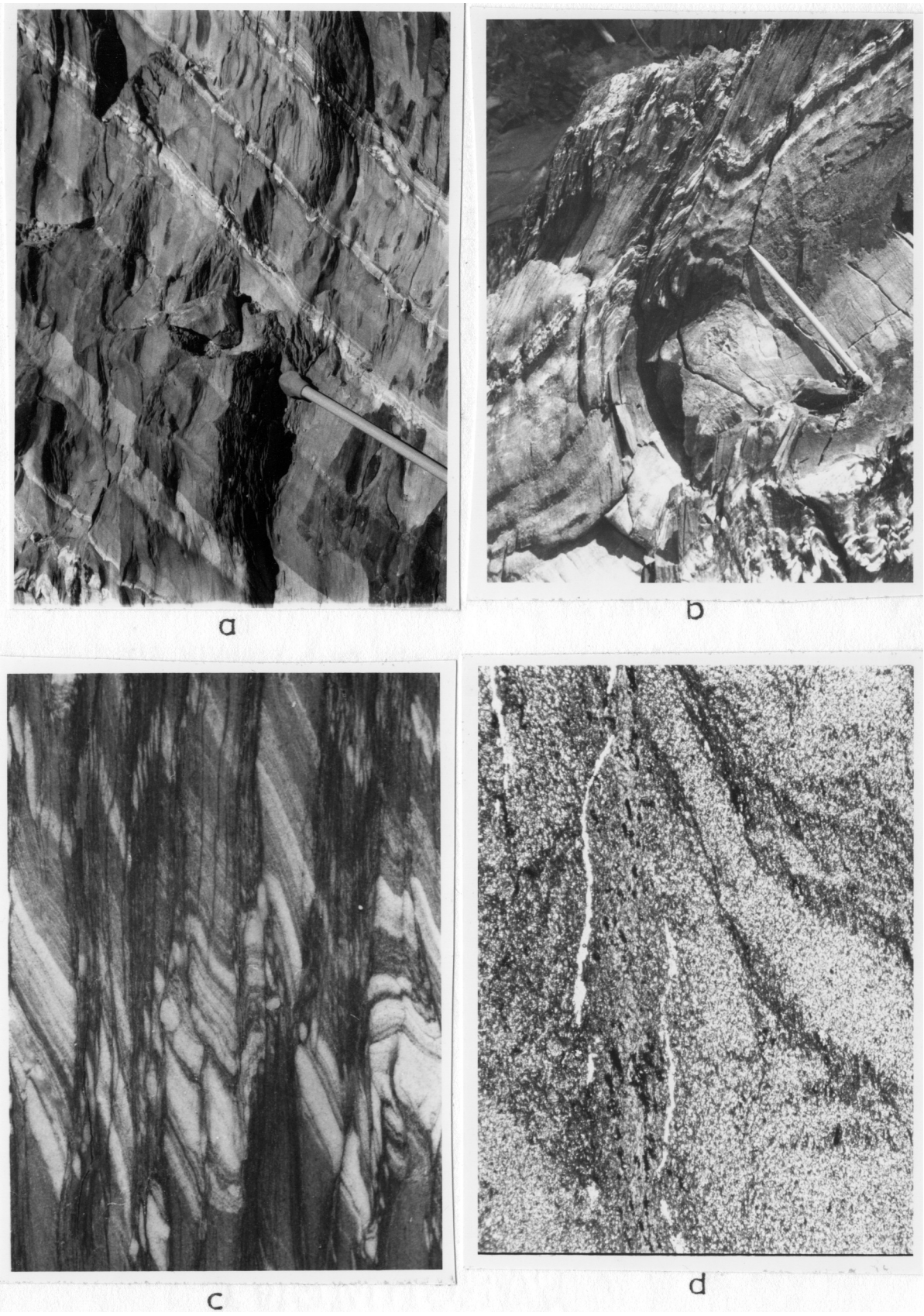

Fig. 1.9

Figure 2.1 - Scanning electron microscope imagery of uncleaved siltstone specimen S-56 (near Survey Point 29).

a) at 25 X magnification, weak traces of bedding-parallel parting surfaces can be observed (S_0 is vertical). In thin section the bedding parallel fabric consists exclusively of opaque mineral horizons. Mica content of the rock is very low, a fact which undoubtedly contributed to the lack of cleavage development. Width of sample is 3 mm.

b) High magnification image of the right hand edge of Specimen S-56 in (a). The surface dipping steeply away on the left is a parting surface parallel to S_0. Elsewhere little evidence of a cleavage fabric is visible. Large "waxy" luster areas are quartz grains, finer clumps of material are probably Fe-rich opaques and a few platy grains are visible, which may be micas.

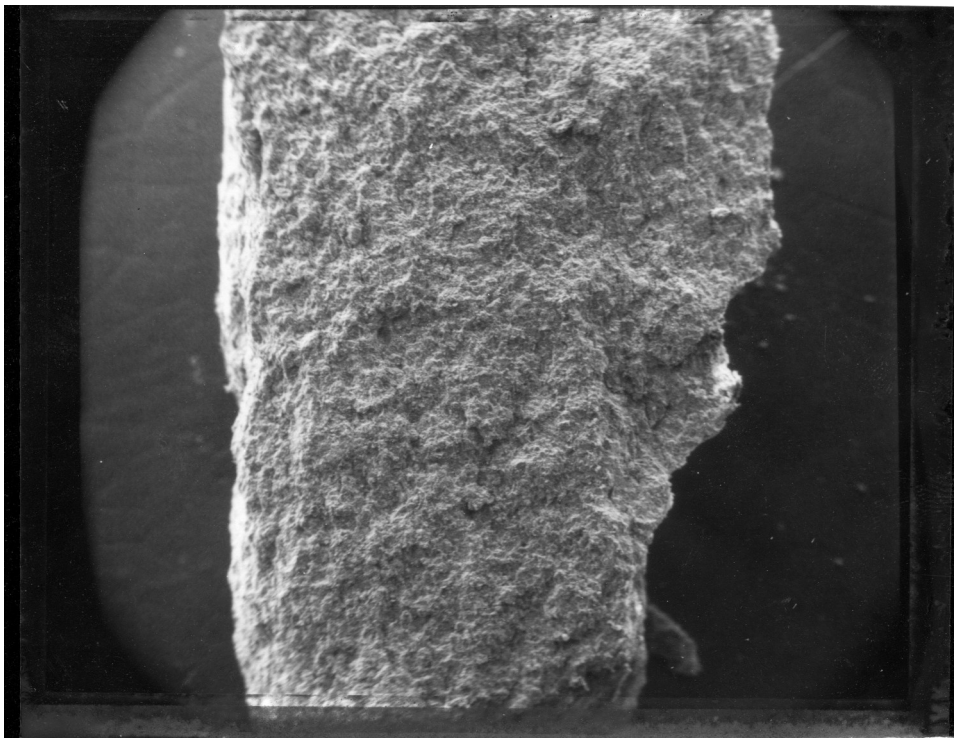

a

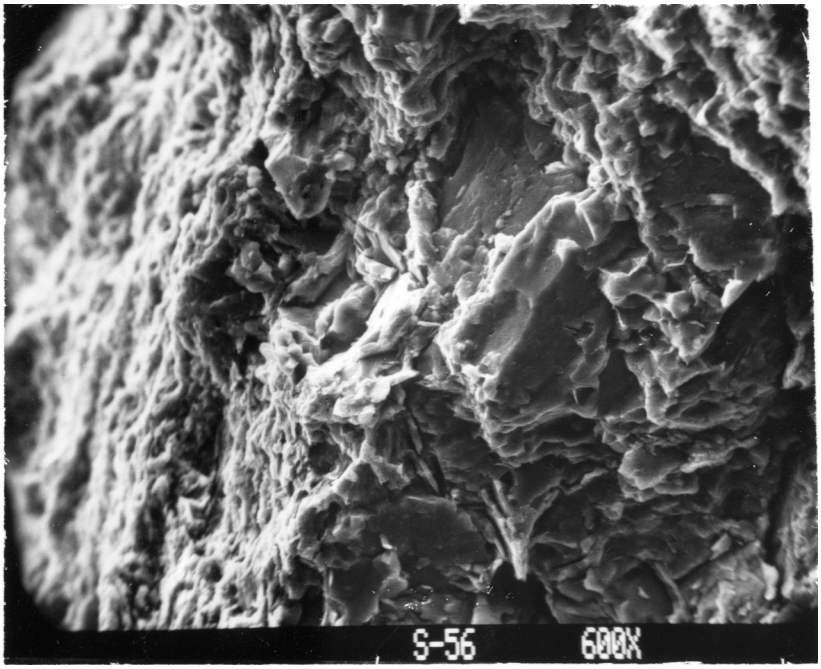

b

Fig. 2.1

Figure 2.2 - Scanning electron microscope imagery of slightly cleaved siltstone specimen S-38. The surface is an irregular fracture perpendicular to bedding and cleavage (S_1). Bright, elongate particles are white mica; large areas with conchoidal fracture surfaces and waxy luster are altered detrital quartz grains.

a) For the most part the photograph consists of quartzo-feldspathic grains of normal "siltstone domains." In the lower left is a large grain which is probably a chlorite porphyroblast. A horizontal film of mica traverses the upper right corner.

b) The center of the preceding illustration is shown at high magnification and typifies material from siltstone microlithons. Secondary quartz rims are indicated by the presence of molds of white mica on quartz grain surfaces. Cleavage is absent.

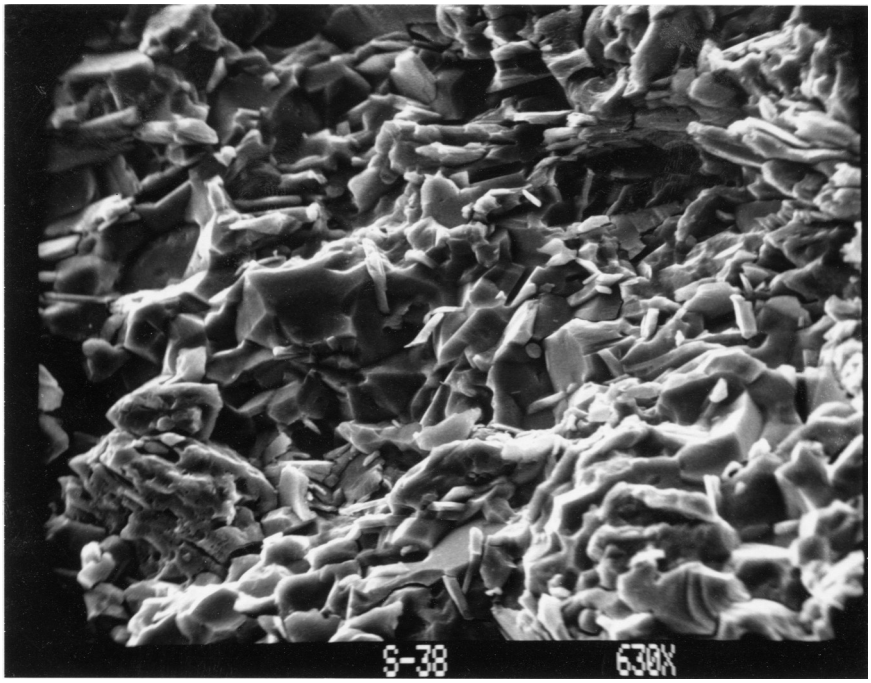

a

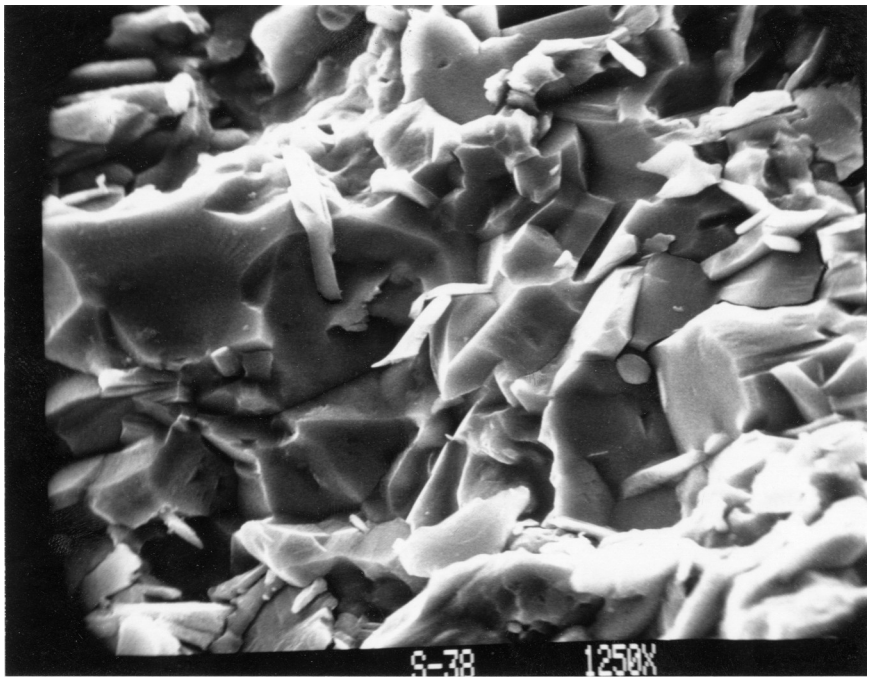

b

Fig. 2.2

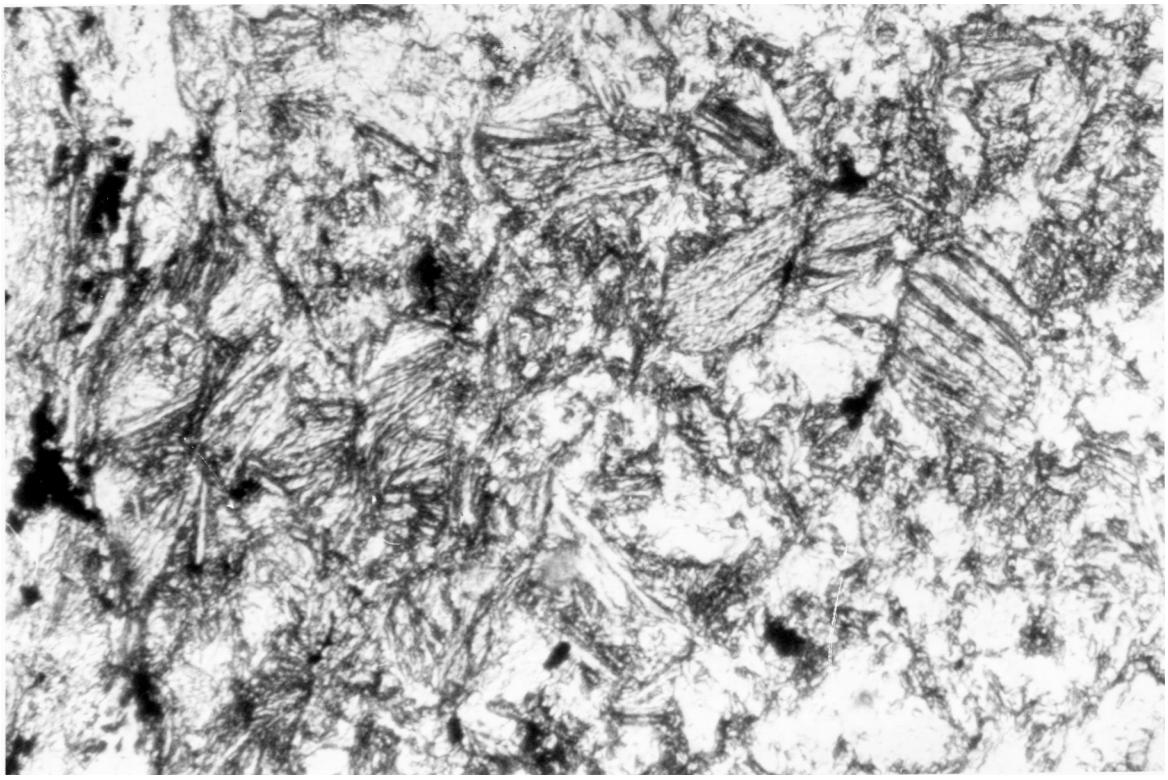

Figure 2.6 - Typical inter-layered chlorite-white mica porphyroblasts of a pelitic lamination within a cross-bedded siltstone. The trace of cross-bedding is horizontal in the photograph. The mesoscopic setting of this layer is illustrated in Figure 2.7a. The open fracture running vertically on the left hand margin marks the boundary between the secondary mica-rich domain and the siltstone microlithions as depicted in Figure 2.7a. Width of photo is approximately 1 mm. Specimen S-32.

Figure 2.7 - Interlayered chlorite porphyroblasts in siltstones.

a) View of pelite horizon shown in detail in figure 2.6. A thick mica-rich secondary layer is shown on the left and the chlorite-rich pelitic bed terminates against the boundary of the domain. Within domains such as this one can often observe large, completely altered remnants of the chlorite porphyroblasts which can be noted by the presence of their inclined (001) traces. Of interest are the opaque minerals within the M-domain. The concentration of opaques is higher in the secondary layer, but the grain sizes and shapes do not differ from those opaques within the siltstone microlithon. This supports the idea that they are of a residual origin (refer to text). Width of photo is about 2.5 mm.

b) Detail of a pelitic horizon from siltstone S-40, showing deformed chlorite porphyroblasts with (001) traces in an "off cleavage" orientation (see also figures 2.10 and 2.11). Short mica film segments, lengthened mica films, and individual cleavage parallel mica particles are visible in the surrounding silty layers. Width of photo is about 1.5 mm.

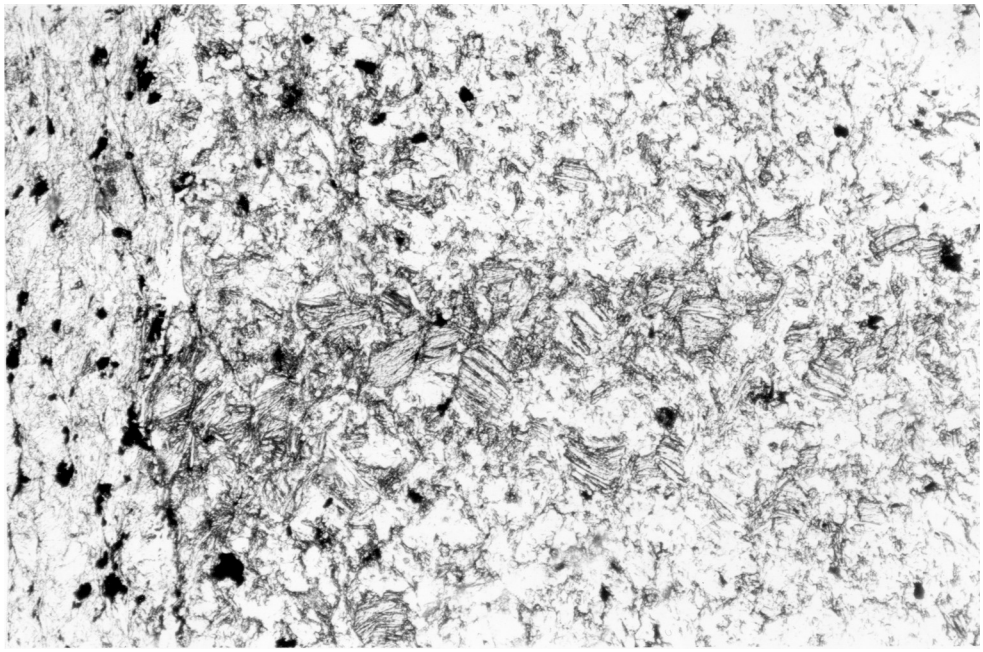

a

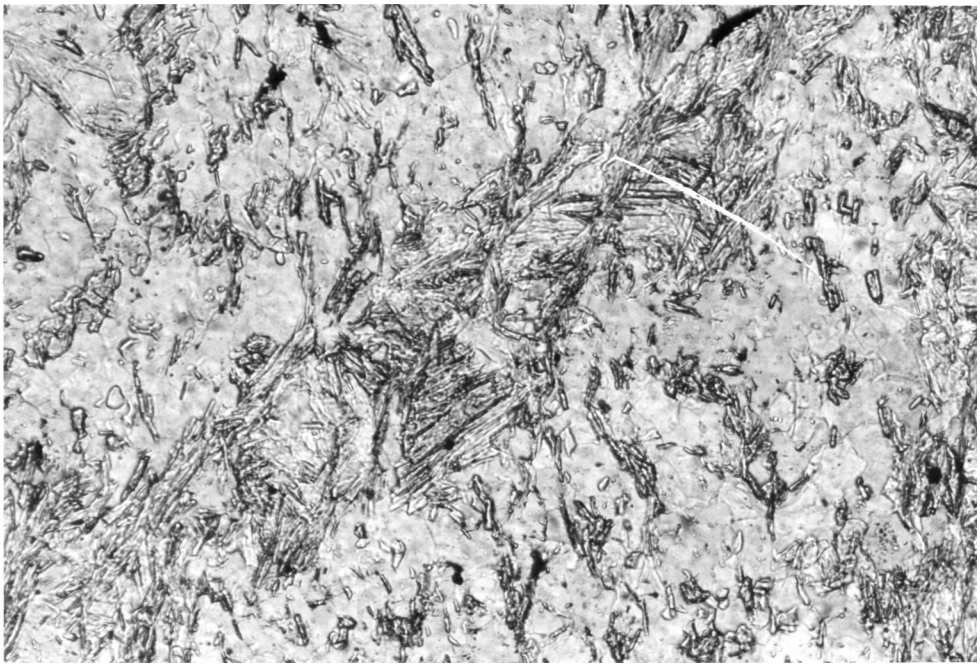

b

Fig. 2.7

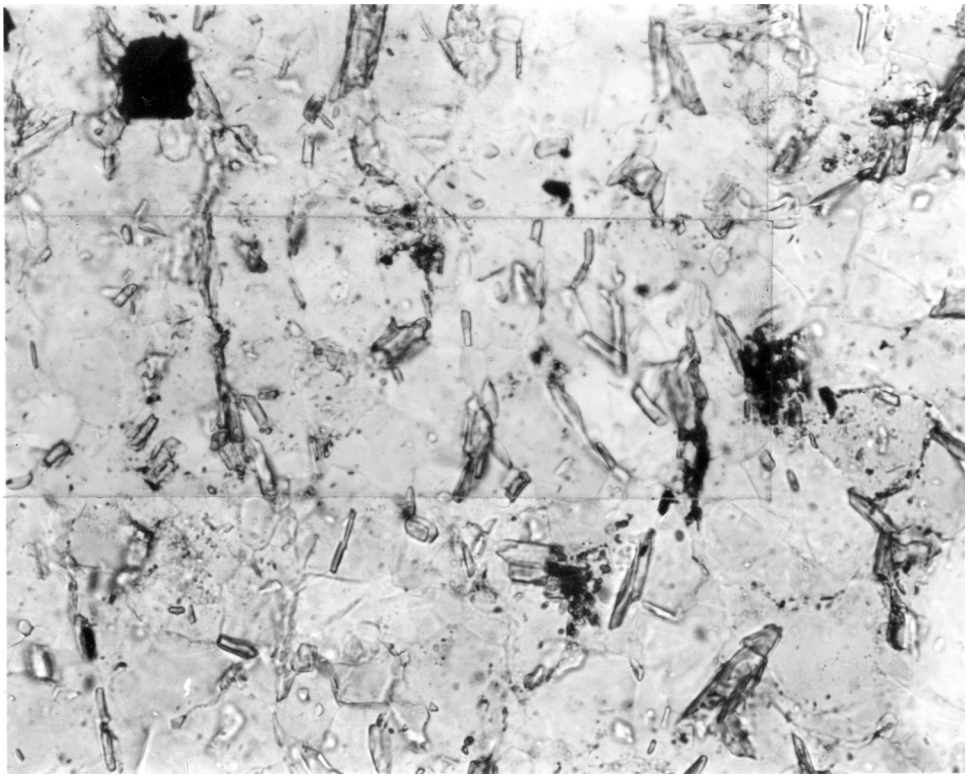

Figure 3.2 - Detail of short film segments. In this example some of the recrystallized white mica is organized into short films of single grain thickness. In the center of the photograph are a few films about 4 or 5 grains long. The lengths of these segments are about the same as the long dimension of the clastic grains which they are in contact with. On the left side of the photograph a longer mica film is developed. Specimen S-33 of siltstone bed I at Turtle Head. Width of photo is about 0.4 mm.

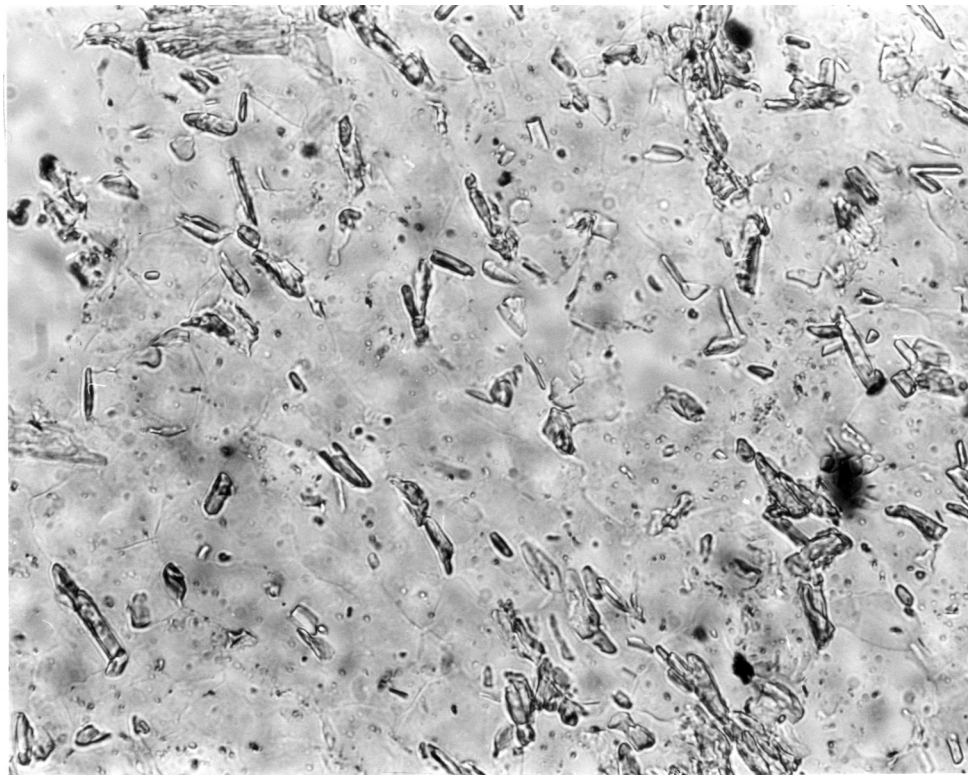

Figure 3.4 - Specimen S-31 of siltstone bed I (site BM, Turtle Head). Characteristic texture of weakly foliated siltstone containing no well developed M-domains. Foliation is defined predominantly by oriented, individual mica plates. Crystallization of clay minerals along quartzo-feldspathic grain boundaries during tectonism could be responsible for this texture. Preferred orientation of micas may be controlled by the dimensional alignment of detrital grain contacts which have been modified from their initial shapes, perhaps by a solution-transfer process. S_0 to S_1=65°; S_1 is oriented from lower right to upper left. Width of photo is about 0.4 mm.

Figure 3.5 - Microstructural detail of a short film segment (x-nicols in lower photograph). A typical film is shown just left of center. The film is about 3 or 4 grains long and one grain thick. Note that the length of short film segment is about the same as the long dimension of the clastic plagioclase grain in contact with it. Other micas in the photograph are single grain and randomly oriented structures presumably crystallized from clay minerals along detrital grain boundaries. Specimen S-28 from bed I at Turtle Head. Width of photo about 0.2 mm.

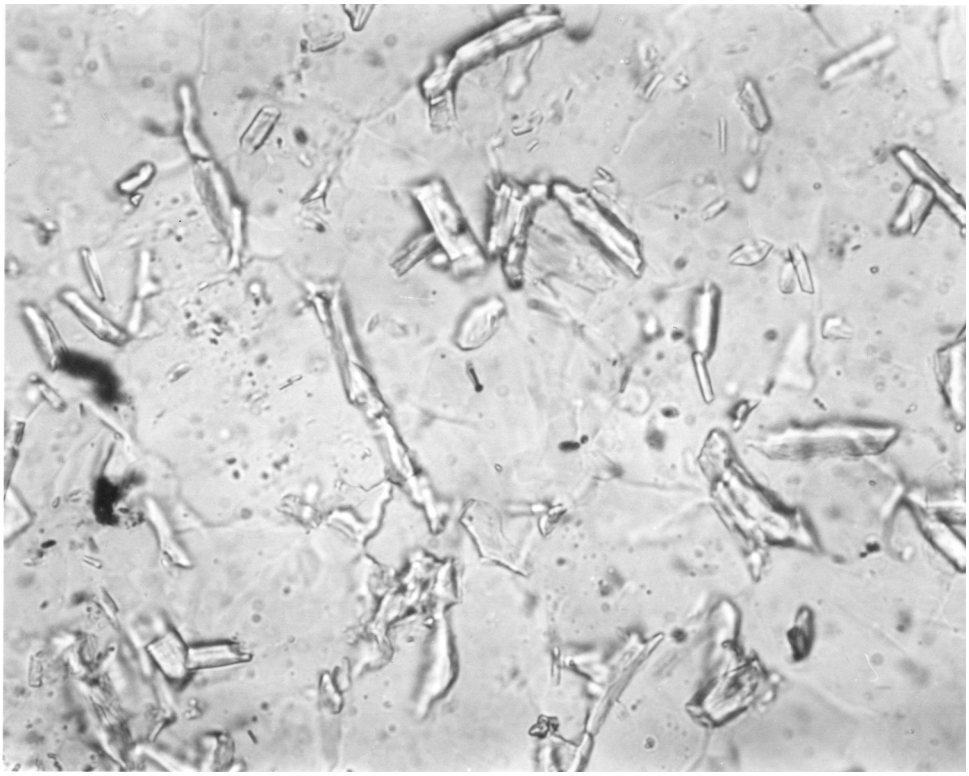

a

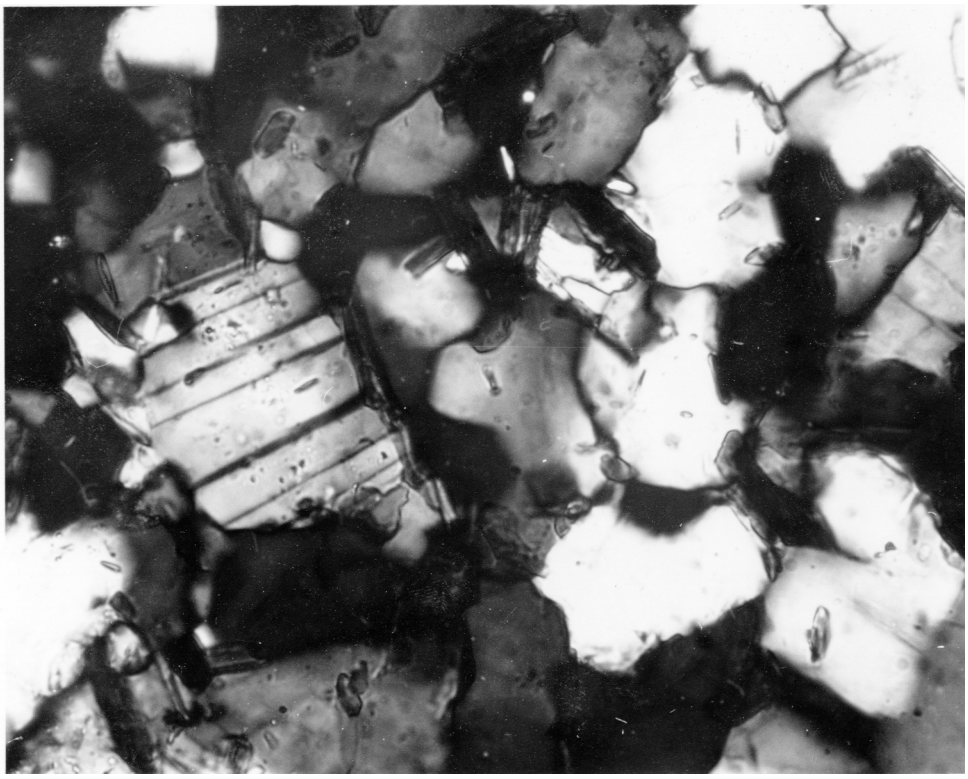

b

Fig. 3.5

Figure 3.7 - Detail of a typical lengthened mica film. Most of the film is 2 or 3 grains thick and tens of grains long. These films often split or diverge into separate films which eventually terminate and show typical short film morphology. This can be seen on the left side of the photograph. A few unconnected short film segments can also be observed. The mechanism by which short film segments link to form continuous mica films is not understood and is a fundamental research topic in cleavage study. Specimen S-31 from Bed 'I' at Turtle Head. Width of photo about 0.4 mm.

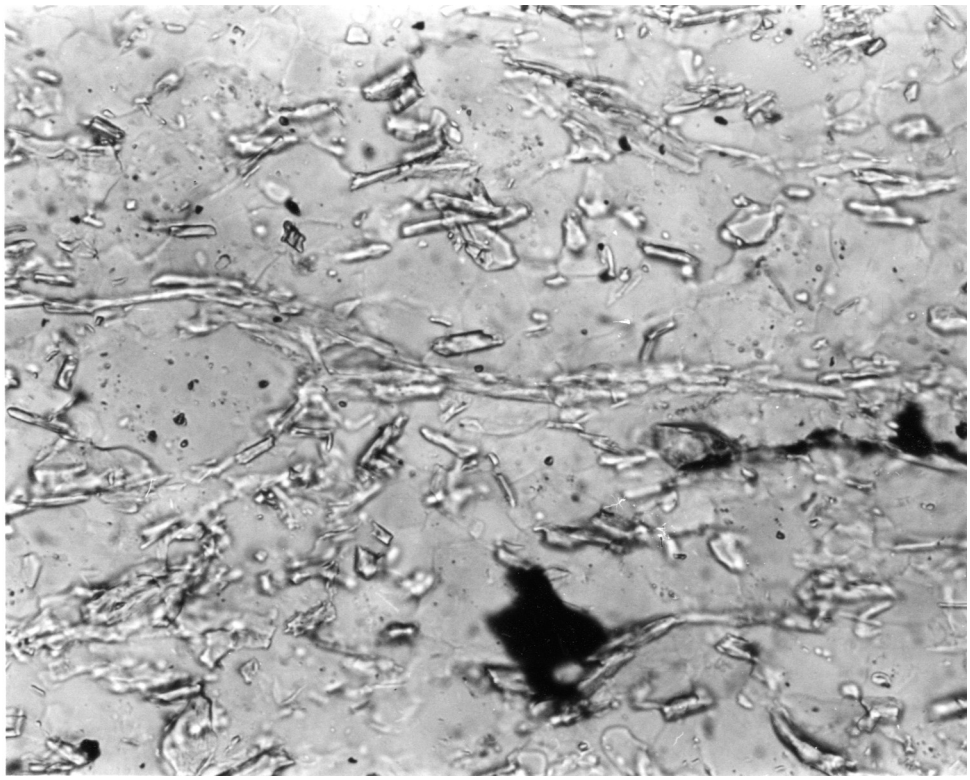

a

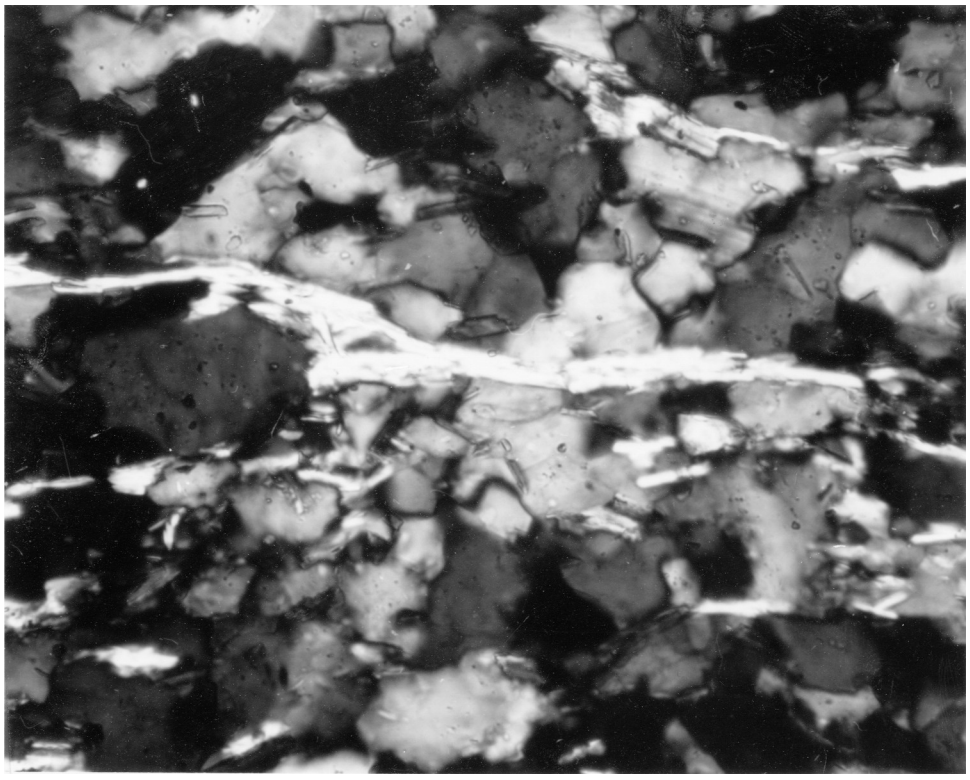

b

Fig. 3.7

Figure 3.8 - Examples of modified lengthened mica films. These photographs illustrate textural changes in mica films resulting from crystallization of micas within thick segments of films. Thin films usually contain fine mica with (001) parallel to the film boundaries. Thick films may show less preferred orientation and larger grain size. This is partly illustrated here by the "cross-micas" lying athwart the film. Thickening of mica films is thought to occur primarily by accumulation of mica during solution transfer removal of quartz along the domain boundaries. The quartz grains abutting mica films always display a "bevelled" appearance along the contact. Coarse grained analogues of the newly crystallized "cross micas" are not found outside of the mica film. Specimen S-28 from bed 'I' at Turtle Head. Width of photo about 0.4 mm.

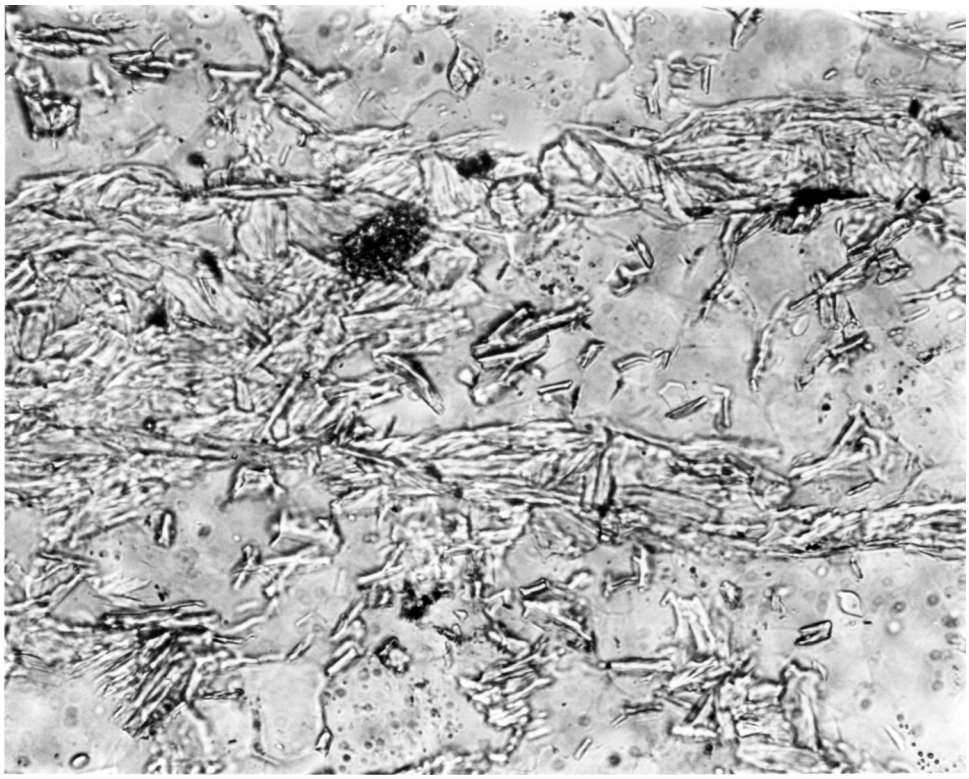

a

b

Fig. 3.8

Figure 3.9 - Scanning electron microscope imagery of siltstone S-38.

a) high magnification photograph of a lengthened mica film and surrounding quartz grains.

b) Iron x-ray distribution image corresponding to the preceeding photograph. The distribution probably reflects the high content of Fe-rich opaque minerals in the mica-films as compared to siltstone microlithons, and is useful in illustrating the overall shape of the M-domain.

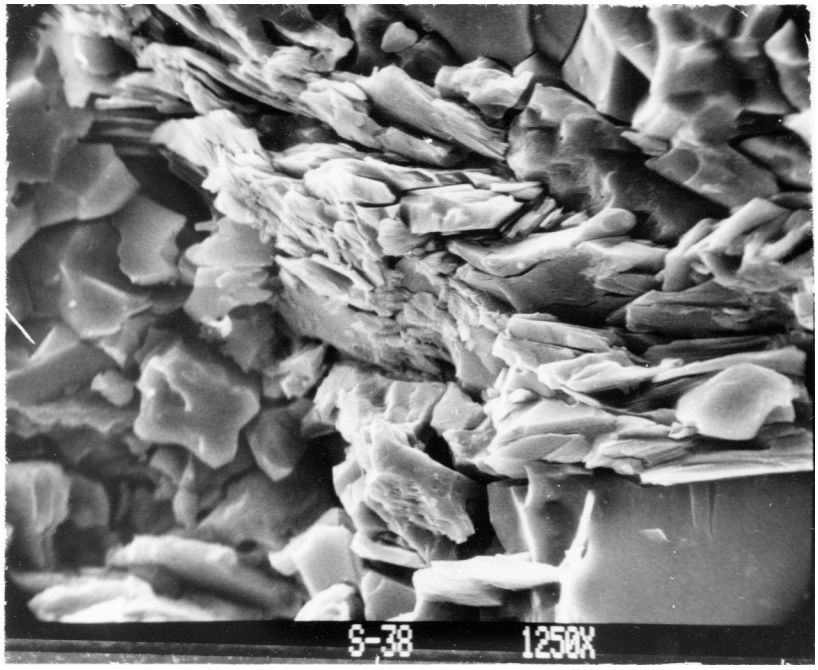

a

b

Fig. 3.9

Figure 3.10 - Microstructure of a typical M-domain.
a) The three largest black areas within the domain are voids produced during grinding. The typically sharp boundaries of the secondary layer are well illustrated. Width of photo about 2 mm.
b) Microstructural detail within the center (white) area of the M-domain in (a). Quartzo-feldspathic minerals are rare in the M-domains. The coarse grained fabric shown here contrasts markedly with the highly oriented fine-grained mica of short film segments and extended film segments. Measurements of (001) in mica for this particular area are shown in Figure 3.11. Specimen S-27 from bed 'I' at Turtle Head. Width of photo about 0.17 mm.

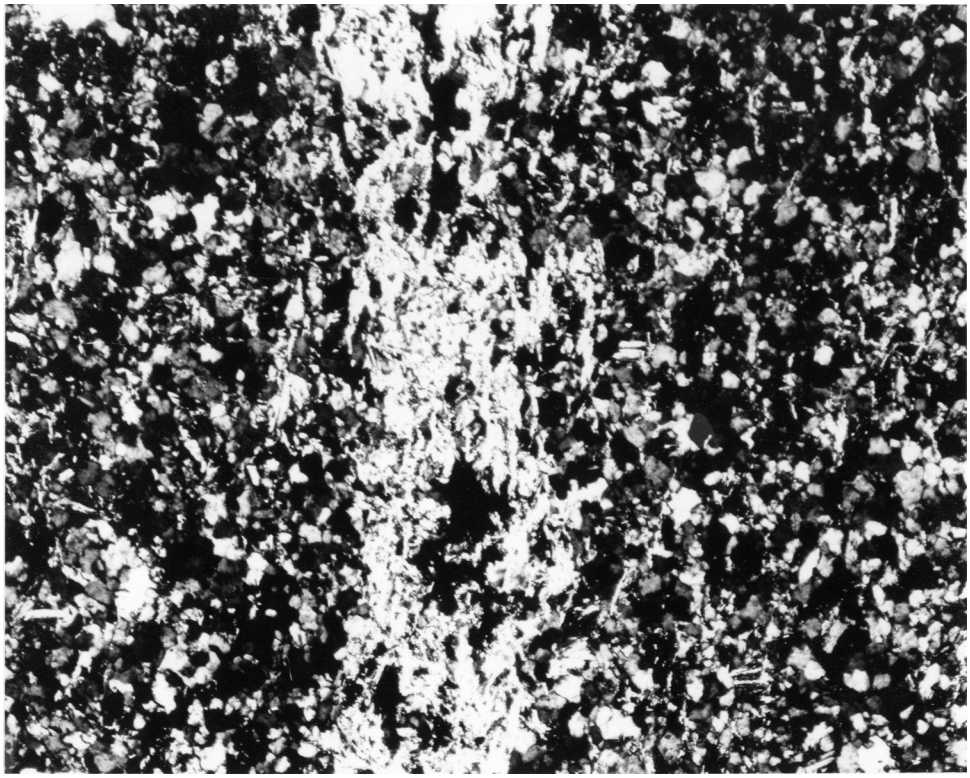

a

b

Fig. 3.10

Figure 3.12 - Accumulation of detrital opaque minerals in cleaved domains. In this specimen (S-27) cross-bedding is marked by placered heavy mineral laminations which run from lower left to upper right in the photo. In the middle of the photo a single cleavage domain runs vertically. Where the cleavage domain and the cross-bedding intersect there is an accumulation of opaque minerals. These opaques show the same grain size and shape characteristics as those in the cross-laminations and appear not to have suffered recrystallization. It is suggested that opaques in the cleavage domain result from the accumulation of residuum during the process of solution transfer of quartzofeldspathic minerals in the areas where cross-laminations border the cleavage domains. Width of photo about 20 mm.

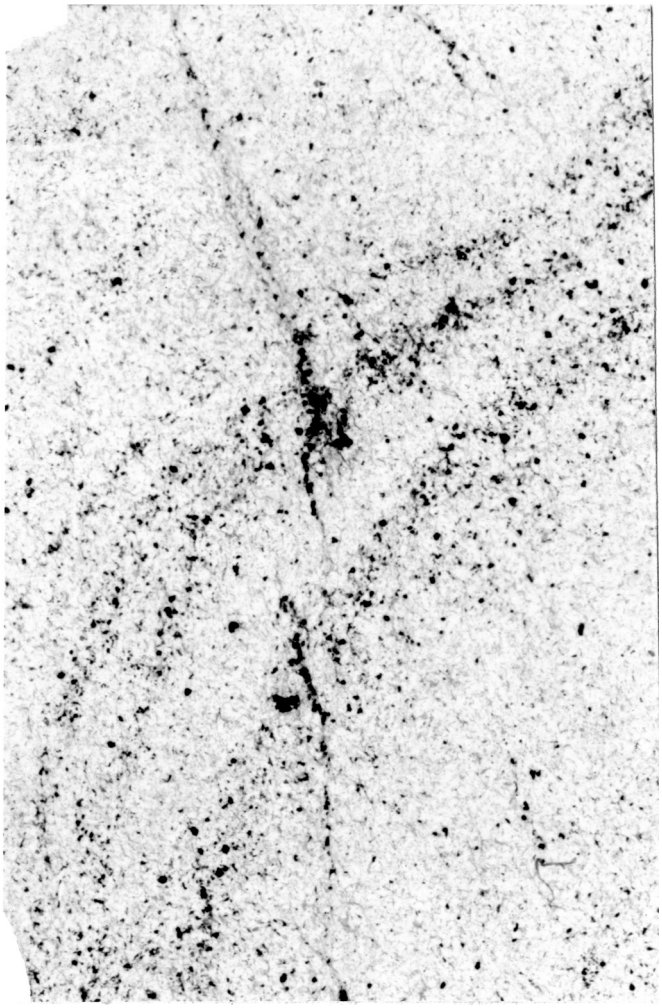

Fig. 3.12

Figure 3.13 - Trace of bedding horizons through thick mica-rich S_1 domain. In this typical example one can easily follow individual pelitic laminations through the secondary layer. This S_1 layer is oriented vertically and encompasses the middle third of the photograph. The domain boundaries coincide with the obvious inflection points in the S_0 layering. In thin section the S_1 layering show higher birefringence color due to the presence of thicker and more abundant white micas. Of additional interest are the horizontal dentate fractures which traverse the S_1 domain and terminate at its boundaries. These fractures are stained bright red-orange in thin section and contain oxide residuum. The origin of these fractures is unknown and they have only been observed in this specimen (S-103). Width of photo is 6 mm.

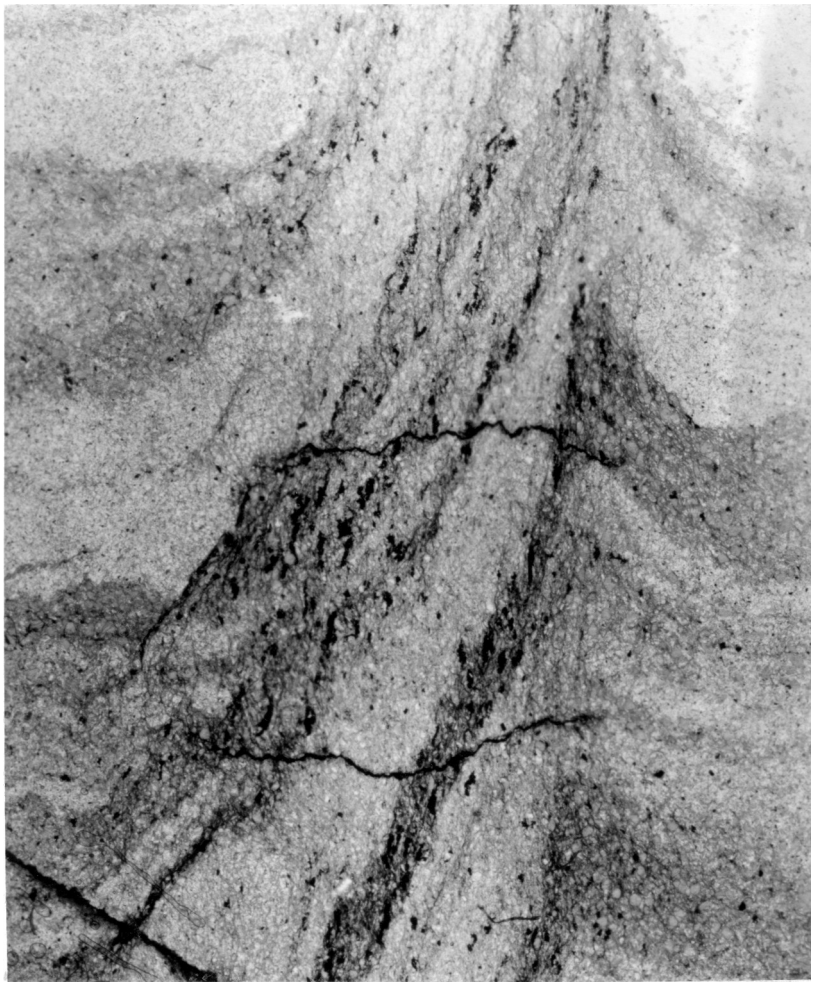

Fig. 3.13

Figure 3.14 - Typical cross-bedded interlayered pelite and siltstone units, specimen S-103. The mica-rich secondary layers oriented vertically in the photograph show terminations ending in relatively "pure" end members of the lithologic sequence. At "s" the layering terminates in a bed composed dominantly of silt and placer deposits of heavy minerals. At "p" the layering terminates in a bed where pelitic material dominates. This behavior is seen on various scales in the Islesboro rocks.

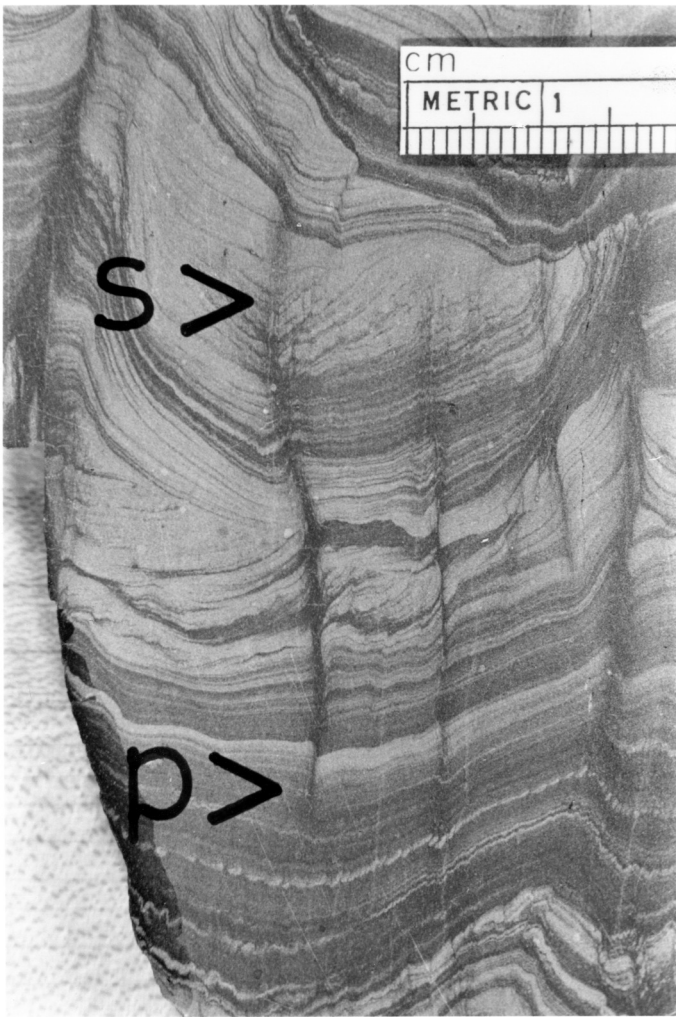

Fig. 3.14

Figure 3.21 - The photograph shows a plagioclase grain which has been cut by a mica film in the immediate region of the film illustrated in figure 3.19. In figure 3.19 a number of quartz grains with nearly coincident c-axes which were situated on opposite sides of the mica film were identified as initially single grains which were fractured during mica film development. The grain illustrated here further attests to this mechanism. The sketch below indicates the position of the grain relative to the mapped area of figure 3.19 on the original rock chip. The distance from the grain illustrated above to the mica film is estimated to be less than 0.1 mm.

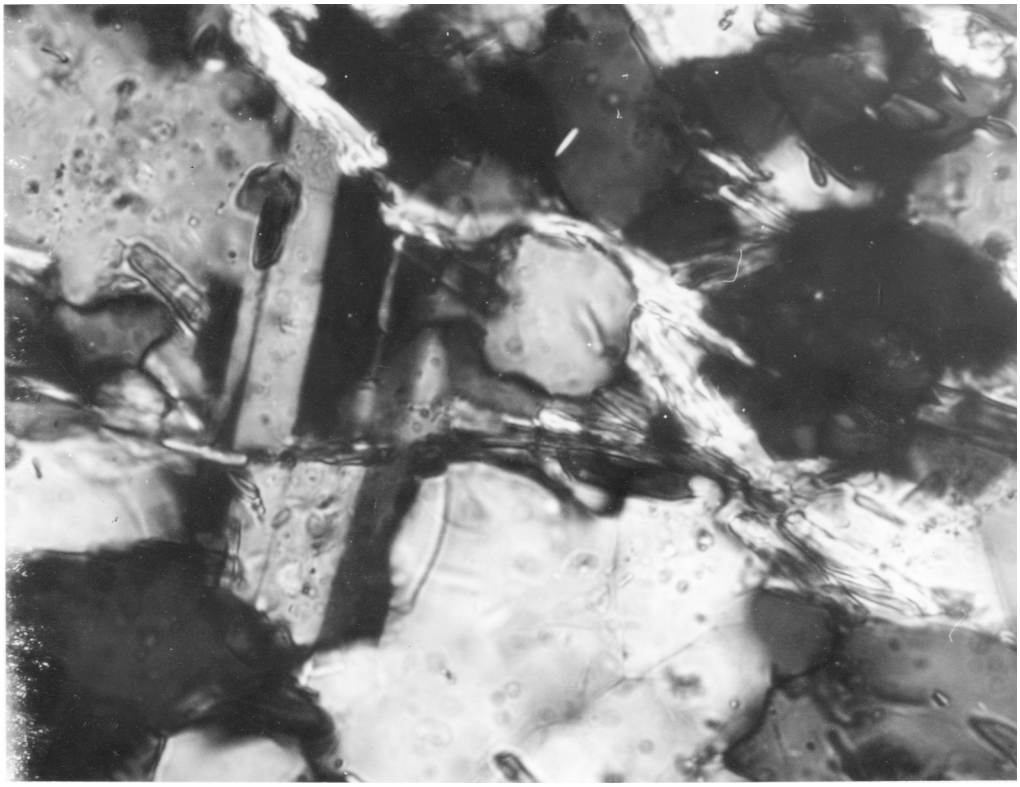

a

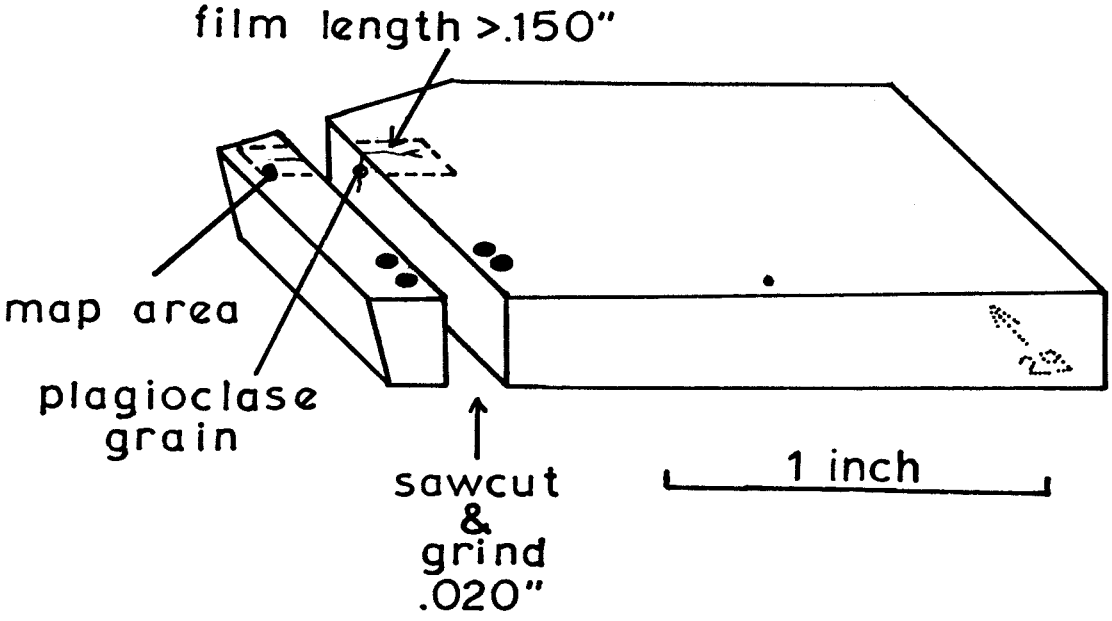
film length >.150"
map area
plagioclase grain
sawcut & grind .020"
1 inch

b

Fig. 3.21

Figure 4.1 - Typical examples of clastic dikes as they appear on the outcrop surface at the New Paltz exposures. The dikes are usually difficult to see because of their size and lack of contrast in color with the surrounding matrix. Dike number 1 shows this well; it is located about 15 cm to the left of the number in the photograph. All of the views show here are in the same relative orientation as the surface labeled "typical outcrop view" in figure 4.2.

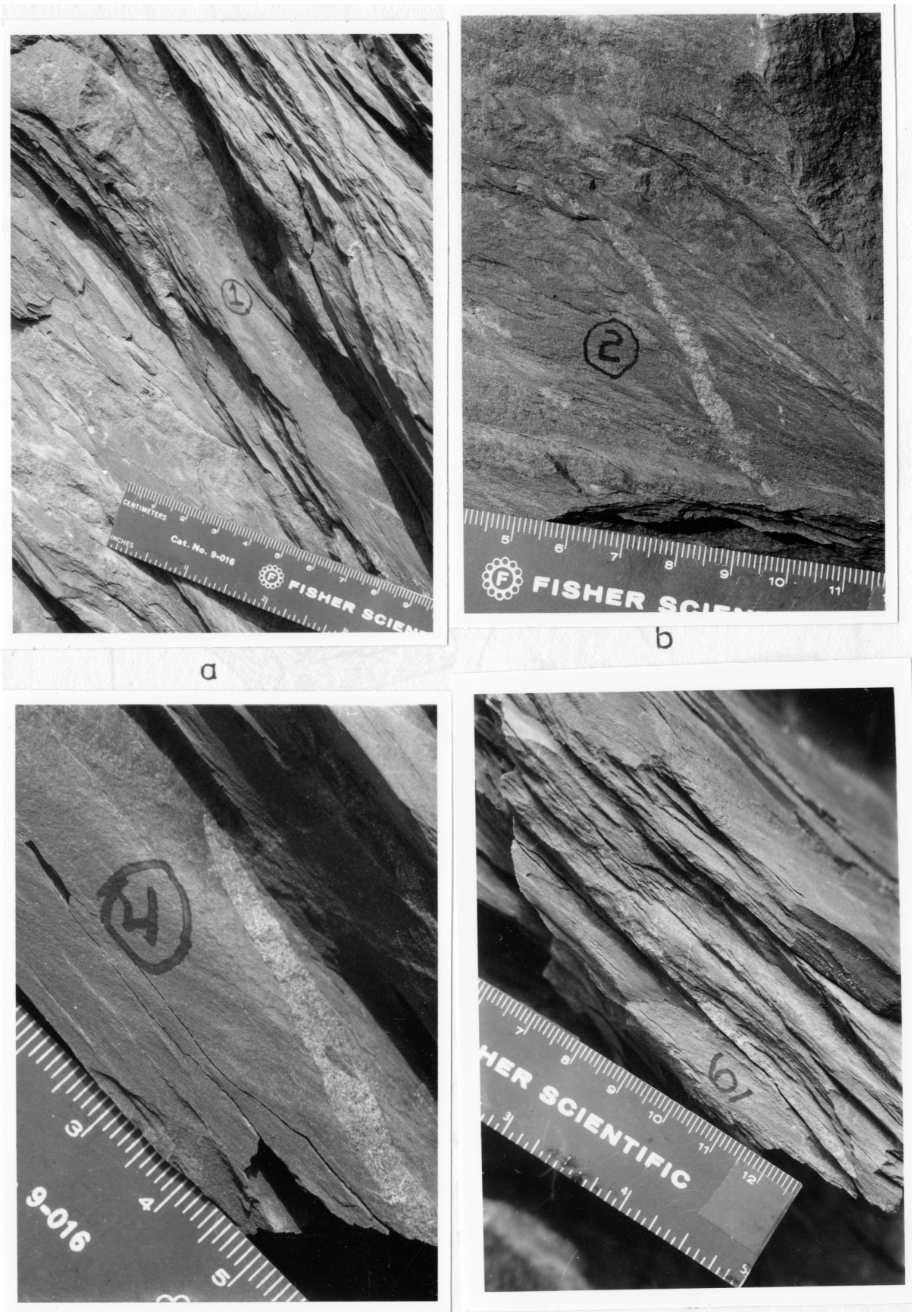
1
CENTIMETERS
INCHES
Cat. No. 9-016
FISHER SCIEN
a
2
FISHER SCIEN
b
4
9-016
61
HER SCIENTIFIC

Fig. 4.1

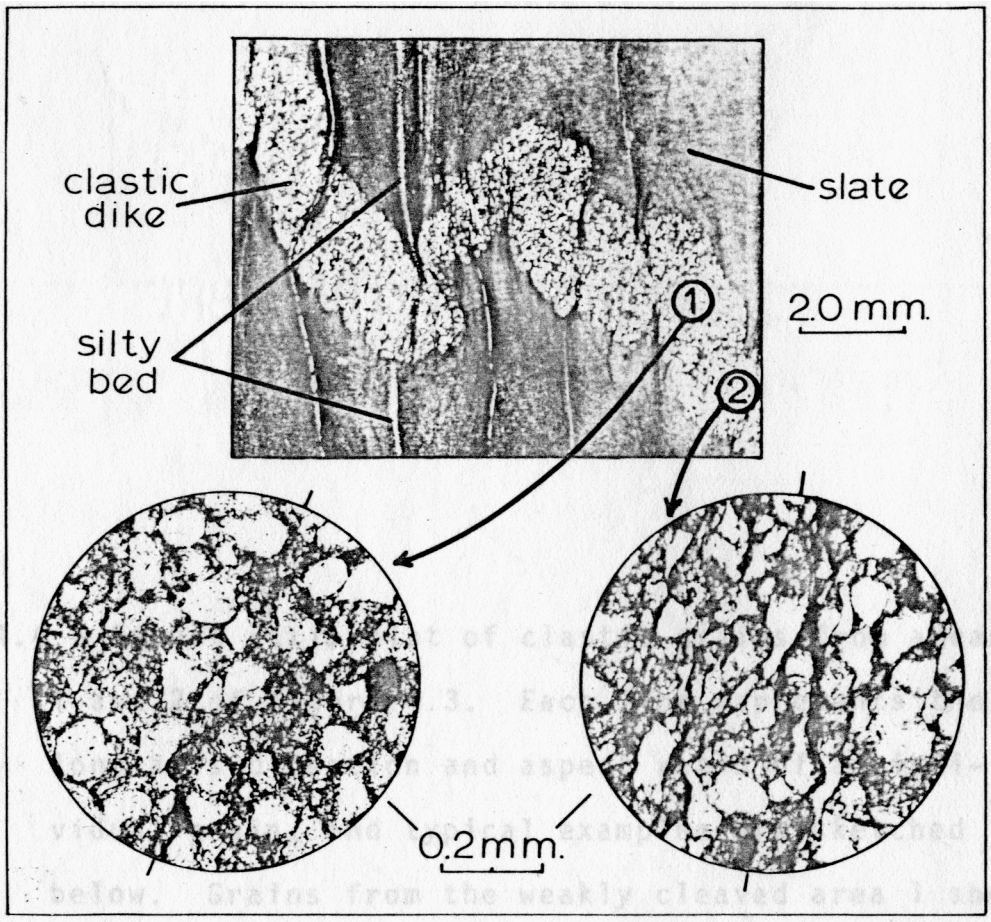

Figure 4.3 - Microstructure of clastic dikes and associated cleavage. The slaty cleavage in the surrounding pelite is continuous with the cleavage in the dike and is an axial surface foliation to the depicted dike folds as well as folds in bedding. Bedding is subparallel to cleavage in this photo and is marked by a thin silty bed. Areas 1 and 2 show corrosion of clastic grains in weakly deformed and strongly cleaved segments of the clastic dike.

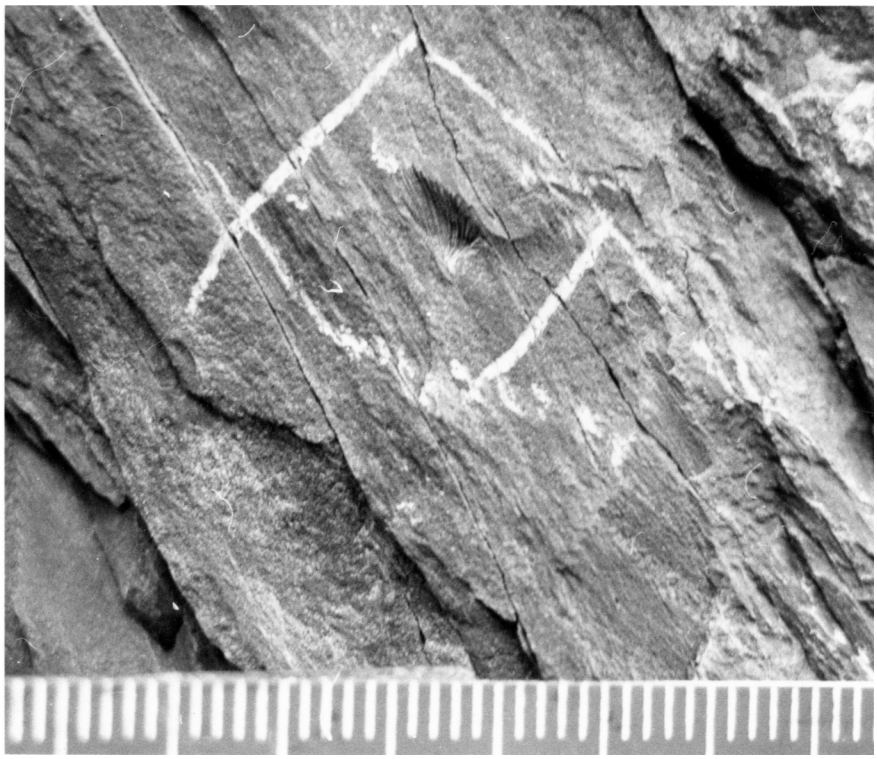

Figure 4.6 - Deformed brachiopod from the New Paltz exposure. This fossil was mentioned but not illustrated in Geiser (1975). The white markings around the fossil were scratched into the slate by a previous visitor. The foliation depicted is slaty cleavage. Geiser (1975) cited the presence of deformed fossils at this locality as supportive evidence against Maxwell's hypothesis. Scale divisions in mm.

Figure 5.2 - Typical appearance of tabular and equant garnet grains.

a) Sketches showing tabular form and bounding quartz veins (see text).

b) Photograph of polished hand specimen showing variation in forms within a single specimen.

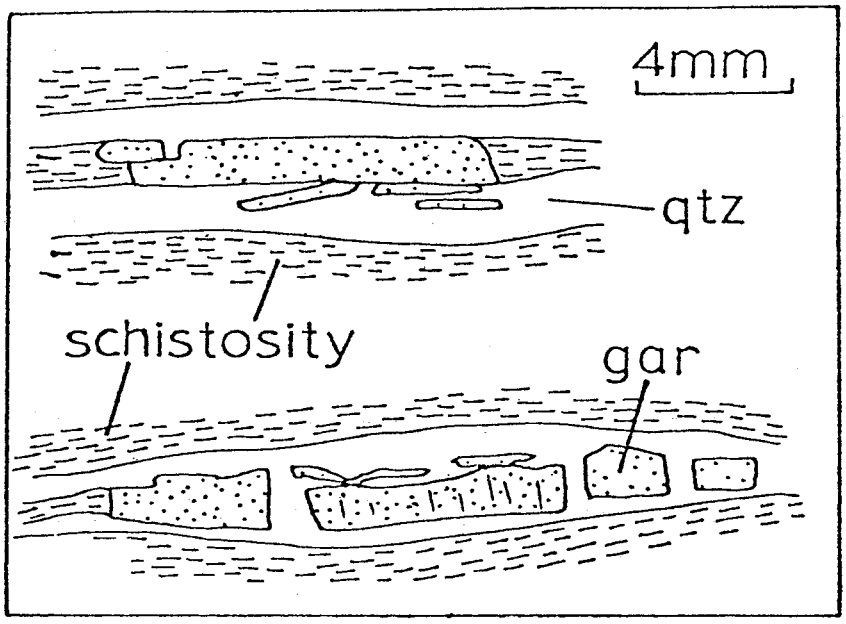

a

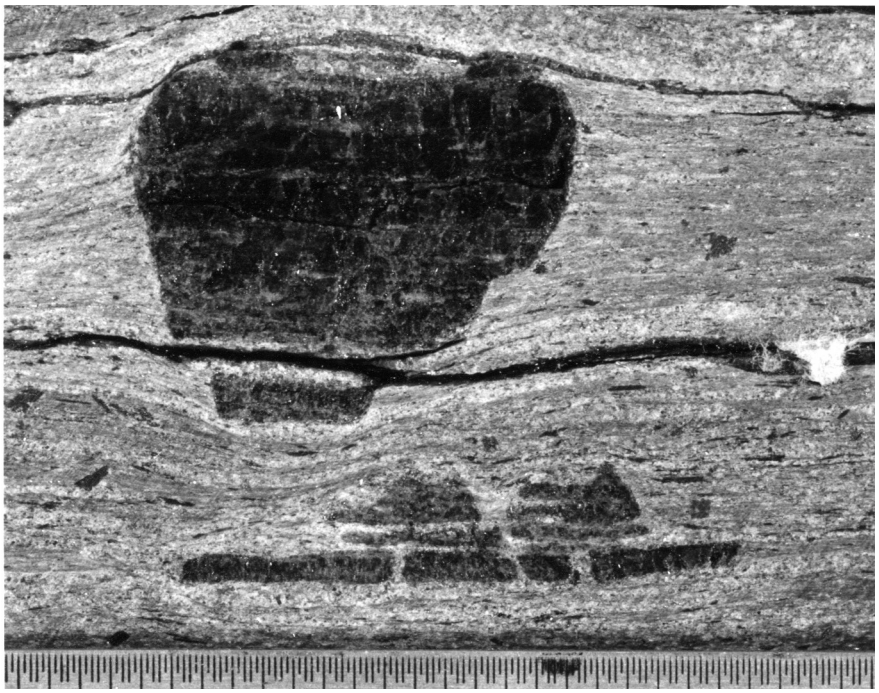

b

Fig. 5.2

Figure 5.3 - Details of garnet grain shape.

a) Photograph of weathered schistosity surface showing equant, idioblastic shape of garnets in this plane.

b) Garnet grains demonstrating shear displacement of initially more equant grain. Specimen is from same rock sample as Fig. 5.2.

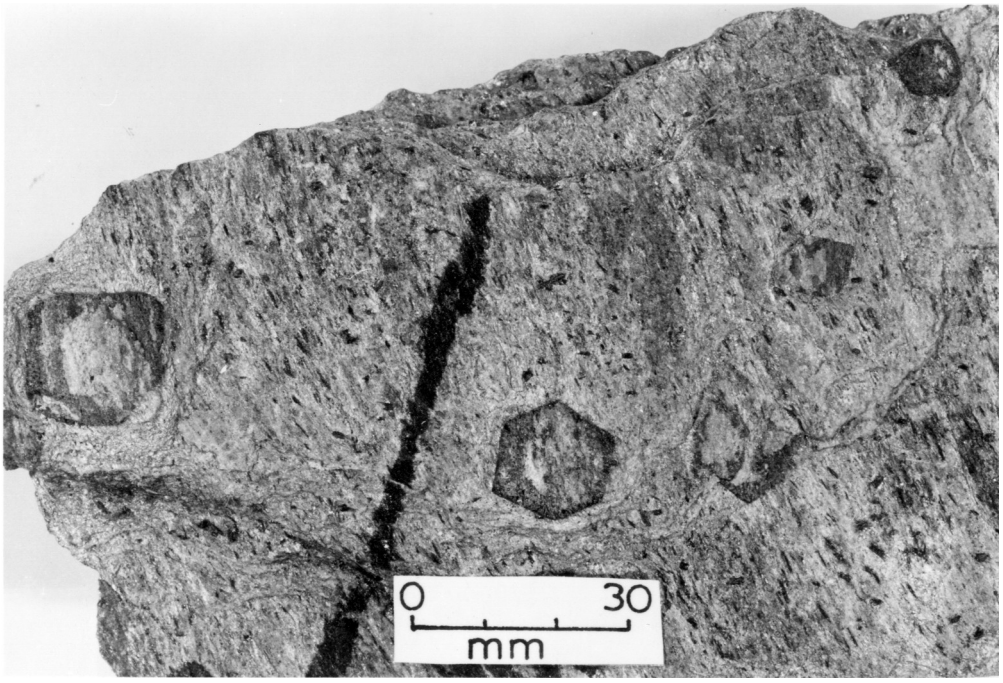

a

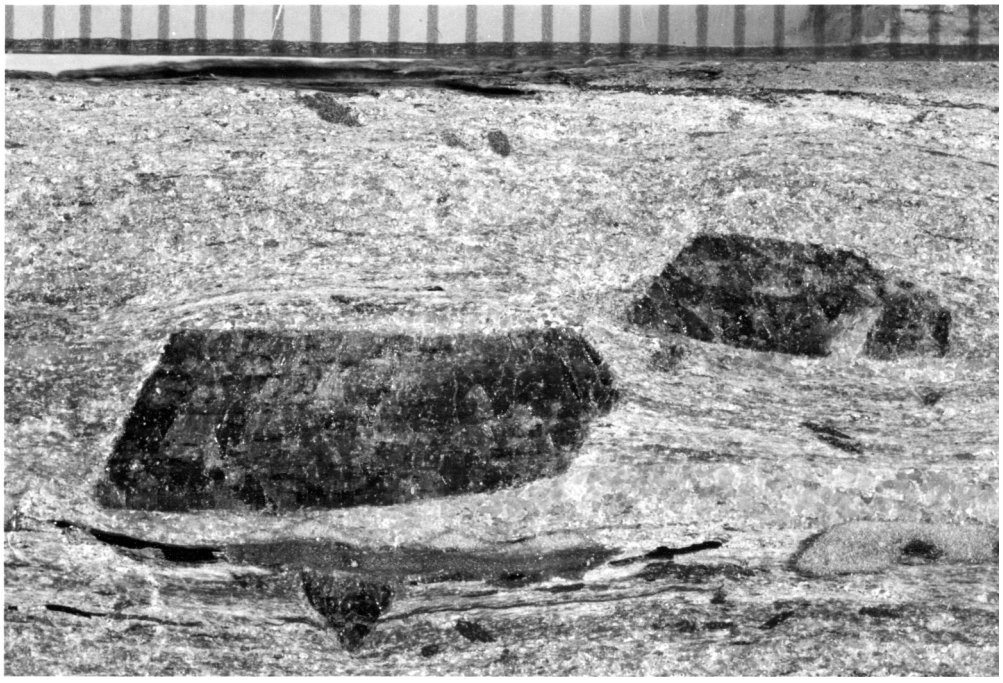

b

Fig. 5.3

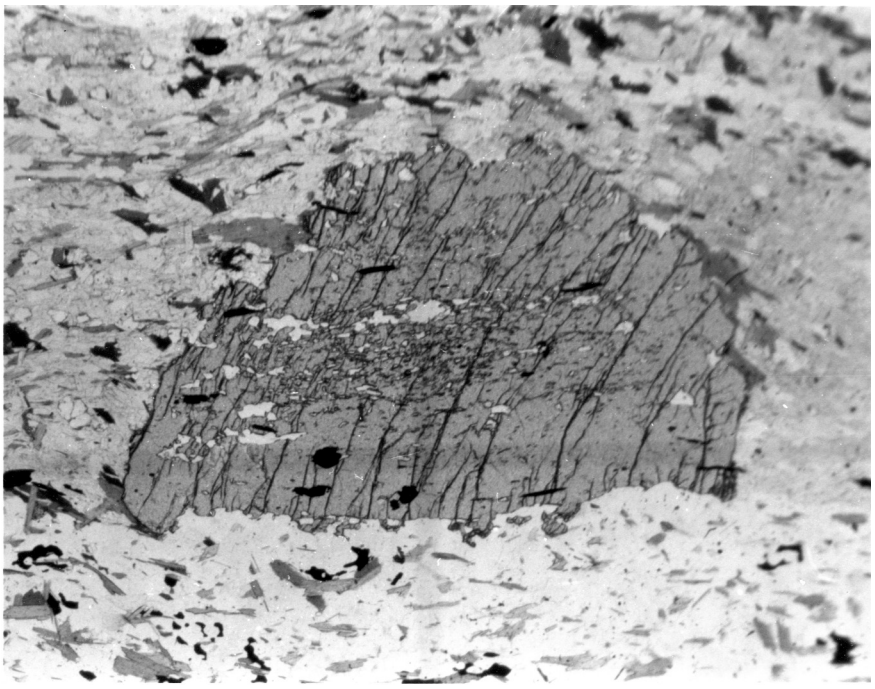

Figure 5.4 - Microstructure of a displaced garnet segment from specimen 6-R-72, 206' showing details of inclusion fabric which may be partly mimetic in the case of opaque minerals and partly deformation-induced in the case of quartz inclusions. Note that quartz veinlets are more abundant in the area above the boundary defined by change in orientation of fractures in garnet. Such fractures are usually not curviplanar in metamorphic rocks (see, for example, studies in Turner and Weiss, 1963, p. 434-435).

Figure 5.7 - Sliced garnets in Adirondack Rocks

a) This illustrates the shapes of garnet crystals when viewed perpendicular to the gneissic layering. The grains are typically idioblastic or equant in this plane. The central crystal is 3 mm in diameter; b) When viewed parallel to the gneissic layering, the crystals are typically tabular in form and rarely show idioblastic shapes. The large crystal is 5 mm long.

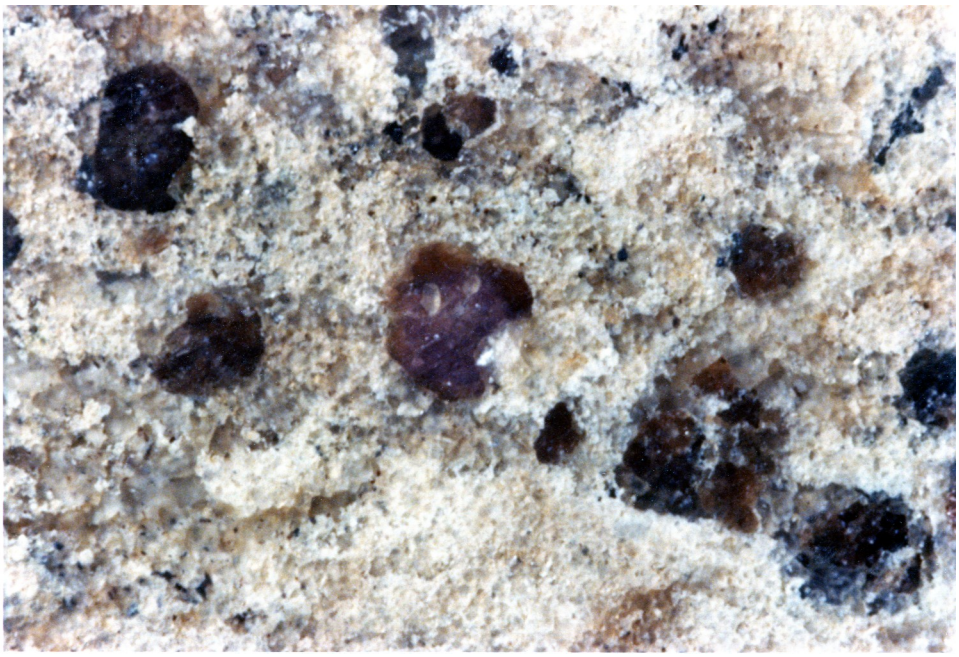

a

b

Fig. 5.7

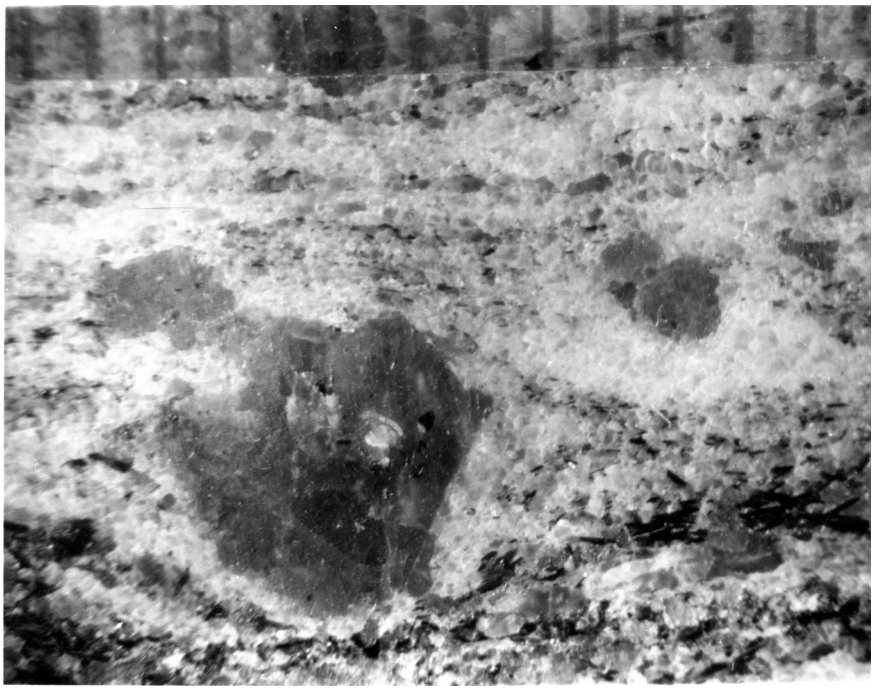

Figure 5.8 - a) Sliced garnet crystals in a quartzo-feldspathic gneiss from Overlook, New York in the southeastern Adirondacks. Both garnet grains appear to have been sliced near their top halves, possibly along the same displacement surface.

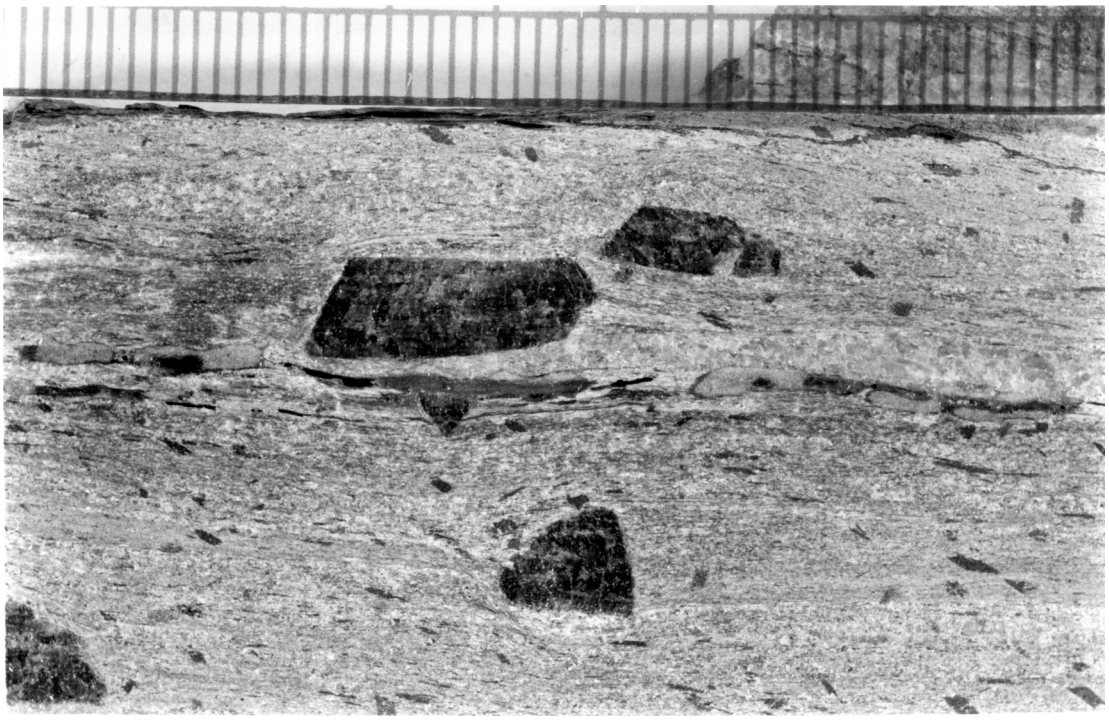

Figure 6.1 - Tabular garnet grains in a chlorite-muscovite schist from Vermont, U.S.A. The grains have been formed by the slicing of initially idioblastic garnets parallel to schistosity. The surfaces along which grains have translated are marked by quartz-rich layers with minute fragments of garnet (see Gregg, 1978). Cross-micas that pre-date this schistosity and the subsequent slicing appear as small black grains oriented diagonally from right to left in the photograph. These cross-micas parallel an earlier foliation and their traces along the schistosity surface are illustrated in figure 6.2. The scale markings are in mm.

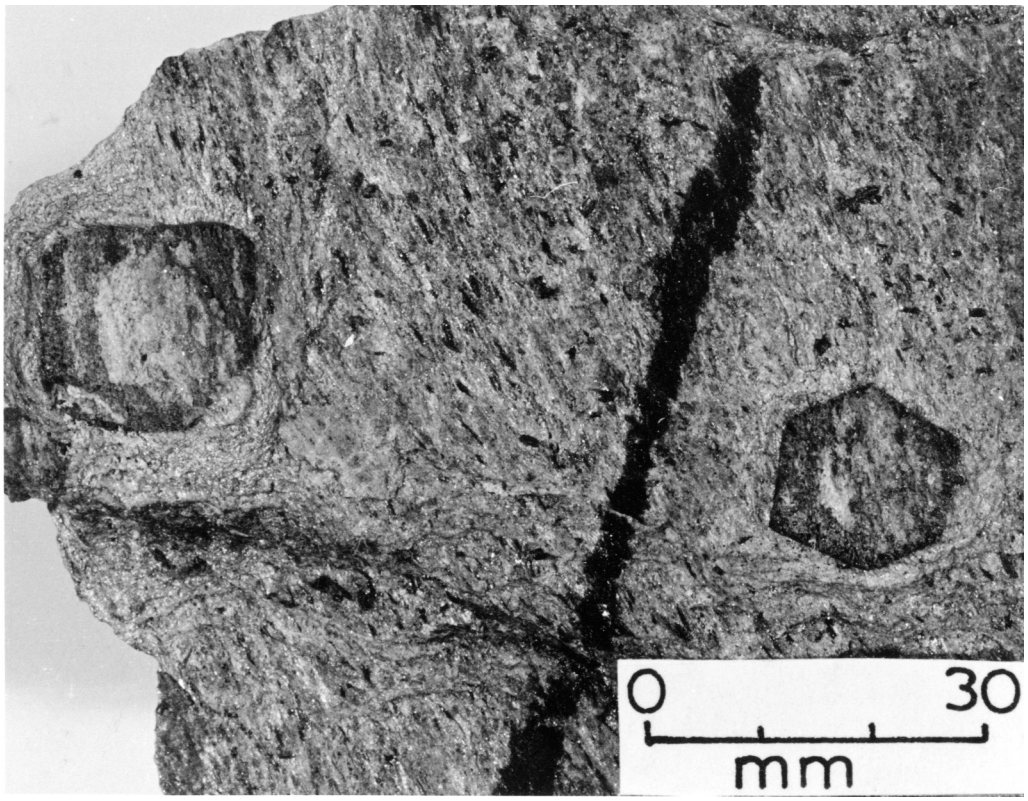

Figure 6.2 - Schistosity surface of the specimen illustrated in figure 6.1, showing idioblastic shape of garnets in this view and edge-on views of small cross-biotites which define the lineation (L_2) in the Moretown schists and finely laminated gneisses Measurements of the traces of these cross-micas relative to the overall trace of L_2 are shown in Figure 6.3. The heavy black line is a portion of an orientation symbol.

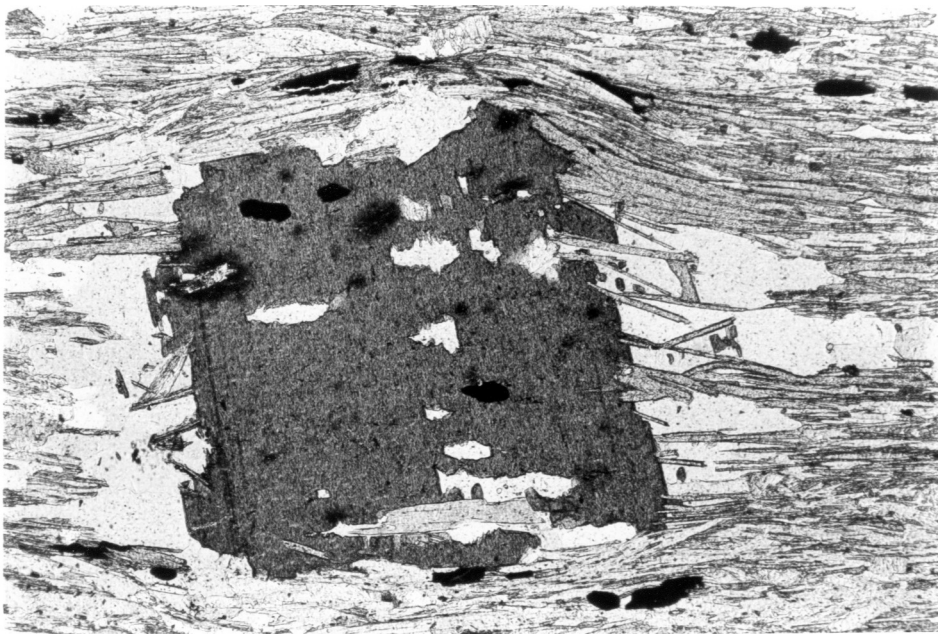

Figure 6.4 - Microtexture of a slightly deformed cross biotite illustrating well developed "pressure shadows" of quartz, penetration of the porphyroblast by fine micas in the late schistosity, and deflection of the schistosity around the edges of the cross-biotite. These textural elements are indicative of an early, pre-tectonic origin of the cross-biotites (Spry, 1969).

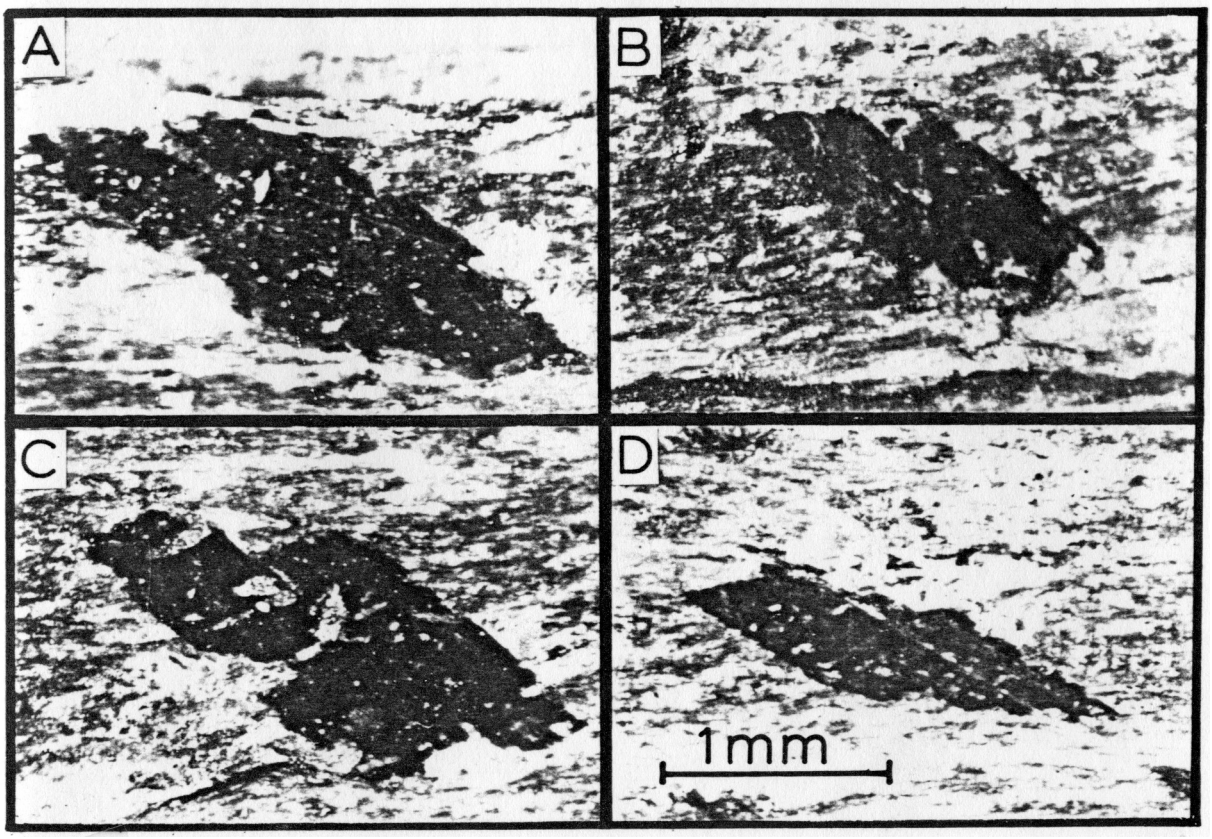

Figure 6.5 - Details of cross-biotites of figure 6.1, illustrating "slipped" appearance common in most grains. Grain 'C' is further illustrated in Figure 6.6 where it has been restored to a more equant form by translation along an (001) plane. Note especially the slipped "card deck" appearance of grain 'D.' Measurements taken by the author consist of the aspect ratio of each grain and the angle β shown as the acute grain boundary relationship in 'A.'

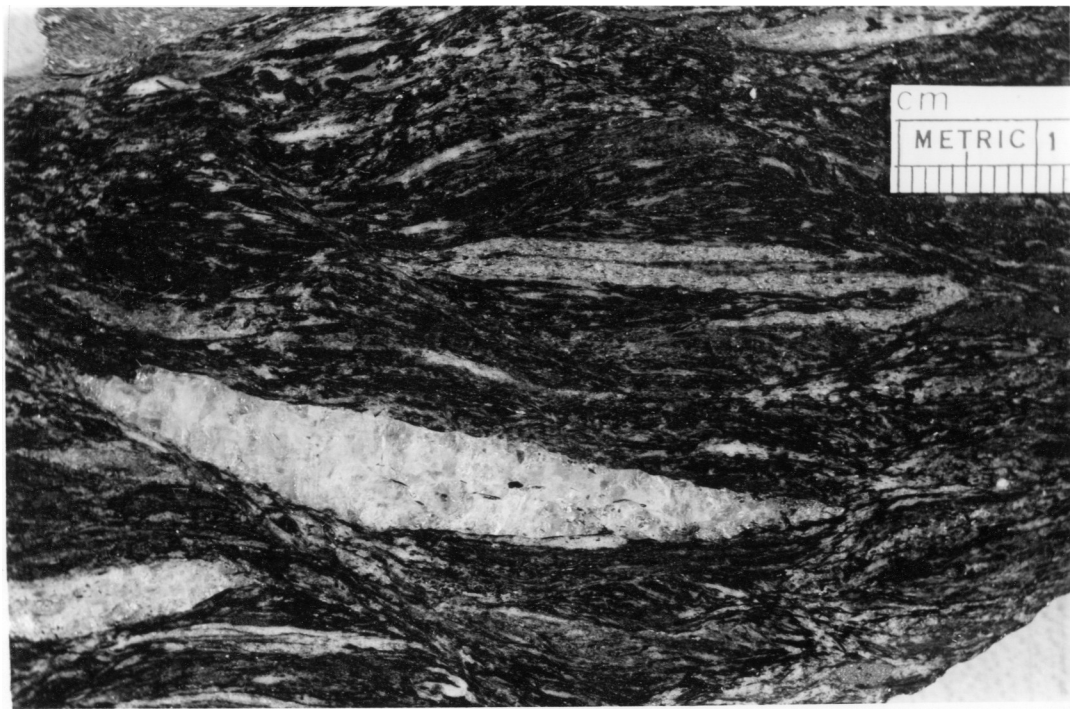

Figure 7.4 - Transposition of early layering in a rock from Springfield, Vermont. This is from the type locality of the Shaw Mountain Conglomerate (Thompson, 1959). Transposition of early layering has resulted in the formation of features resembling pebbles to the casual observer. Closer inspection reveals isolated fold hinges and lensoid remnants of fold limbs characteristic of transposed layering. Microstructural detail of this specimen is shown in figure 7.5.

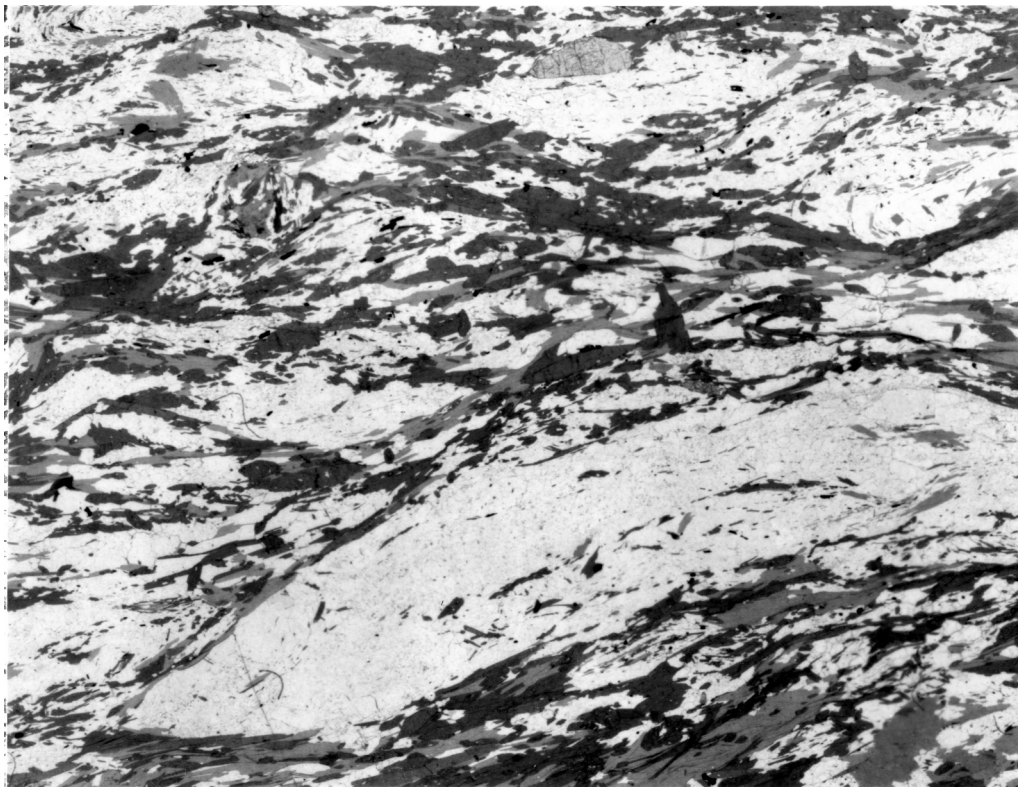

Figure 7.5 - Thin section view in plane polarized light of the Shaw Mountain Conglomerate shown in figure 7.4. The large white lensoid area is composed of quartzo-feldspathic material and is an element of the transposed layering. The matrix material consists of oriented chlorite and green amphiboles. In this example, the competent layers illustrate transposition and the weaker matrix displays a schistosity.